355

Prediction of the US-Storm of 24-26 January 2000 with the ECMWF Ensemble Prediction System

Roberto Buizza and Piero Chessa

Research Department

January 2002
In press in the Monthly Weather Review

For additional copies please contact

The Library
ECMWF
Shinfield Park
Reading, Berks RG2 9AX

library@ecmwf.int

Series: ECMWF Technical Memoranda

A full list of ECMWF Publications can be found on our web site under:
http://www.ecmwf.int/pressroom/publications.html

Abstract

Between the 24th and the 26th of January 2000 explosive cyclogenesis along the US East Coast caused serious economic disruption and loss of lives. The performance of the European Centre for Medium-Range Weather Forecast (ECMWF) high-resolution TL319 model and of the TL159 Ensemble Prediction System (EPS) in predicting the storm evolution is investigated.

The most critical time period to predict was the rapid intensification of the storm between the 24th and the 25th of January. Single deterministic forecasts based on the TL319 model gave skilful predictions only 36-h before the event. By contrast, the EPS indicated the possibility that the storm hit the affected region two days before the event, consistently enhancing the indications present in forecasts issued three and four days before the event. This suggests that the ECMWF EPS, suitably used, could be a valuable support tool for critical issues as alerts for extreme winter weather.

Sensitivity studies indicate that stochastic perturbations added to the model tendencies had a substantial positive effect on the skill of some EPS members.

1. Introduction

Human activities have become increasingly vulnerable to weather: population and infrastructures continue to grow in areas exposed to extreme weather events such as flooding, strong winds and extreme temperatures (*Easterling et al.* 1999, *Kunkel et al.* 1999). Extreme events are often associated with very energetic phenomena (e.g. hurricane, intense storms) during which errors in the initial conditions (*initial uncertainties*) could grow very quickly and affect the forecast accuracy (*Lorenz* 1969, *Ehrendorfer et al* 1995). Furthermore, *model uncertainties* due to the discrete representation of the system equations could enhance the forecast error growth. These two sources of error can lead to inconsistent deterministic forecasts started on consecutive days, thus making difficult to issue extreme-weather warnings.

More sophisticated prediction systems capable of forecasting the time evolution of the probability density function (PDF) of forecast states should be used in these cases. The prediction of this PDF is possible theoretically and can be achieved by integrating the analogous (in numerical weather prediction) of the Fokker-Planck equation for the PDF (*Gleeson* 1966, *Epstein* 1969). Unfortunately, the Fokker-Planck equation and its perfect-model equivalent, the Liouville equation, are only tractable for very simple systems (*Ehrendorfer* 1994a, 1994b), but are intractable for the currently used high-resolution weather prediction models, due to the very large number of degrees of freedom of the system (*Palmer* 2000).

Ensemble prediction provides a practical tool for estimating the PDF of the forecast state using multiple integration of the model equations. Since 1992, ensemble prediction systems have become part of the operational numerical weather prediction practice at the European Centre for Medium-Range Weather Forecast (ECMWF, *Palmer et al.* 1993, *Molteni et al* 1996), at the National Centers for Environmental Prediction (NCEP, *Toth & Kalnay* 1993, 1997) and at the Canadian Meteorological Center (CMC, operational since 1995, see *Houtekamer et al.* 1996). Currently, both the ECMWF and the CMC ensemble systems are designed to simulate the effect of both initial and model uncertainties.

Ensemble prediction can be helpful in forecasting the risk of damage due to extreme weather events: it can be used to attach a level of confidence to a single deterministic forecast and to estimate the probability of occurrence of any event. This latter aspect is particularly important in case of severe weather events (*Petroliagis et al.* 1997, *Buizza & Hollingsworth* 2002).

The prediction of the explosive cyclogenesis that caused serious disruption and the loss of lives on the US East Coast between the 24th and the 26th of January 2000 is considered in this work. A typical case of explosive cyclogenesis (*Manobianco* 1989, *Carlson* 1991), this storm was characterized in the early stages by a surface pressure drop of about 1 hPa per hour and by heavy snowfall over part of East Coast of US. This storm was not properly forecast by single deterministic forecasts issued by ECMWF and by NCEP until 36 hours in advance. This type of storms occurs several times per year (about 6 storms per year, see Fig. 10.9 in *Carlson* 1991) with disastrous effects on coastal areas. Forecast success is case dependent and forecasts of storm intensity are frequently wrong (*Mullen & Baumhefner* 1994).

The rapid evolution of these systems is due to a combination of synoptic and mesoscale factors, among which strong sea-surface temperature gradients play a fundamental role (*Sanders & Gyakum* 1980). In fact the Pacific and Atlantic regions influenced by the Kuroshio Current and the Gulf Stream are the areas most affected by explosive cyclogenesis. Lack of data in those areas, the inherent numerical approximation of moist processes and the fast error growth typical of explosive systems are some of the reasons of the forecast failures in predicting such events.

In this work, predictions given by the ECMWF T_L159L40 Ensemble Prediction System (EPS) are compared with ECMWF deterministic high-resolution T_L319L60 predictions. These two forecasting systems have a horizontal resolution of approximately 120-km and 60-km, respectively, and thus forecasts should not be expected to reveal details at scales smaller than these. This inherent limitation should be taken into account when assessing forecast performance.

The paper is organized as follows. In section 2 the configuration of the ECMWF EPS operational at the time of the storm is briefly described. The synoptic situation during the US storm is discussed in section 3. The accuracy of single deterministic and ensemble forecasts is analyzed in section 4. Sensitivity experiments designed to investigate the impact on EPS perturbed forecasts of initial perturbations and stochastic perturbations added to the model tendencies are discussed in section 5. Conclusions are drawn in section 6.

2. Description of the ECMWF Ensemble Prediction System

Routine real-time execution of the ECMWF EPS started in December 1992 with a 33-member T63L19 configuration (spectral triangular truncation T63 and 19 vertical levels, *Palmer et al.* 1993, *Molteni et al.* 1996). Since 1 May 1994, the EPS has been run daily with 12 UTC as starting time.

A major upgrade to a 51-member T_L159L31 system (spectral triangular truncation T159 with linear grid) took place in 1996 (*Buizza et al.* 1998). This spectral resolution is equivalent to a mid-latitude grid-point spacing of about 120 km. A scheme to simulate model uncertainties due to random model error in the parameterized physical processes was introduced in 1998 (*Buizza et al.* 1999a). The number of vertical levels

was increased from 31 to 40 in October 1999, with the extra levels in the planetary boundary layer (*Teixeira* 1999).

Schematically, each EPS forecast e_j is generated by integrating the perturbed model equations

1) $$\frac{\partial e_j}{\partial t} = A(e_j,t) + P_j'(e_j,t)$$

starting from perturbed initial conditions

2) $$e_j(t=0) = e_0(t=0) + \delta e_j(t=0)$$

where A and P' identify the contribution to the full equation tendency of the non-parameterized and parameterized physical processes. For each grid point $\boldsymbol{x}=(\lambda,\phi,\sigma)$ (identified by its latitude, longitude and vertical hybrid coordinate), the perturbed parameterized tendency P' (of each state vector component) is defined as

3) $$P_j'(e_j,t) = [1+ < r_j(\lambda,\phi,t) >_{D,T}]P(e_j,t)$$

where P is the unperturbed diabatic tendency, and $<..>_{D,T}$ indicates that the same random number r_j has been used for all grid points inside a DxD degree box and over T time steps. The random numbers are currently sampled uniformly in the interval *[-0.5,0.5]*, the same random number is used inside 10° *degree* boxes ($D=10$), and the set of random numbers is updated every *6 hours* ($T=6$) (note that random numbers do not vary with the vertical coordinate σ).

In Equation (2) $e_0(t=0)$ is the operational analysis at $t=0$, while δe_j denotes the j-th initial perturbation. For each day d, the initial perturbations are defined using the singular vectors that grow in the forecast range between day d and day $d+2$ at initial time and the singular vectors that had grown in the past between day $d-2$ and day d at final time

4) $$\delta e_j(t=0) = \sum_{i=1}^{25}[\alpha_{i,j}\nu_i^{d,d+2}(t=0) + \beta_{i,j}\nu_i^{d-2,d}(t=48h)]$$

where $\boldsymbol{\nu}_i^{d,d+2}(t=0)$ is the *i-th* singular vector growing between day d and $d+2$ at time $t=0$ (*Barkmeijer et al.* 1999). The coefficients $\alpha_{i,j}$ and $\beta_{i,j}$ set the initial amplitude of the ensemble perturbations, and are defined by comparing the singular vectors with estimates of analysis errors (*Molteni et al.* 1996).

It is worth mentioning that following extensive experimentation the EPS horizontal spectral truncation was increased from T_L159 to T_L255 in October 2000 (*Buizza & Hollingsworth* 2002).

3. Synoptic description

Figure 1 shows the observed total precipitation (in mm of equivalent water, Fig. 1a,b) and snowfall accumulated between 12 UTC of the 24th and the 25th and of the 25th and the 26th (Fig. 1c,d). The observed

precipitation grid-point field has been constructed by averaging station values inside 1.25 degrees boxes (as in *Mullen & Buizza* 2001; observed precipitation data were kindly provided by Dr S Mullen). Observed snowfall values are shown for stations archived in the ECMWF database and located along the US East Coast that reported snow-depth measurements at 12 UTC of the 24th, 25th and 26th (snowfall is reported in mm of equivalent water and has been computed from snow-depth measurements).

Surface temperatures along the US East Coast are about 0°C degrees on the 25th and below zero on the 26th with a strong gradient along the coast between land and sea (Fig. 1e,f). Average precipitation fields indicate grid-point maxima between 20 and 30 mm (Fig. 1a), with some stations in North Carolina reporting between 30 and 60mm of rainfall between the 24th and the 25th. Precipitation over land started in some locations with snow and ice on the 24th and continued as snow on the 25th and the 26th. The heavy snowfall had serious impact on the East Coast: record snowfall was reported across North Carolina, with Raleigh-Durham (36°N, 78°W) reporting 5cm of snowfall in 4 hours (http://www.emc.ncep.noaa.gov/mmb/research/blizz2000). 10cm of snow depth were recorded at New York La Guardia and 28 cm of snow depth at Baltimore-Washington International (Fig. 1d).

Snowfall verification is not easy since only few stations of the ECMWF archive reported snowfall: one approach could be to analyze the precipitation field in conjunction with the low-level thermal structure, and interpret the precipitation as snowfall wherever below freezing surface temperature is reported. If this approach is followed, then the observed precipitation field between 12 UTC of the 24th and the 25th north of say 35°N (North Carolina, Virginia, Washington area, Fig. 1a) should be considered as snowfall since below freezing temperature are reported for this area (Fig. 1a). By contrast, all the observed precipitation between 12 UTC of the 25th and the 26th should be considered as snowfall since the 0°C 2m temperature isoline runs along the East Coast (Fig. 1f). The other approach would be to consider snowfall only the data reported as snowfall and shown in Fig. 1c,d. Note that there is a good agreement between the observed precipitation and snowfall value, and the thermal structure. This second approach is followed throughout the paper when assessing the accuracy of snowfall predictions.

Although each system has its own peculiarities (*Kocin & Uccellini* 1990), some of the usual features of intensity and duration common to this kind of development (*Carlson* 1991) are present also at this time. On the 24th of January 2000, a surface low-pressure system starts developing to the NorthEast of Florida, downstream of an upper level trough, and in phase with the jet stream axis. At upper levels (not shown) the system evolution is characterized by a strong vorticity advection, in concert with intense cold advection upstream of the surface and warm downstream advection. During the subsequent hours the cyclone intensifies while moving along the strong temperature gradient located between the coast and the edge of the Gulf Stream. Figure 2 shows the storm position at the surface on the 25th and the 26th of January. Between 12UTC of the 24th and 12UTC of the 25th the surface central pressure drops by about 23 hPa, from 1002 to 979 hPa. The surface pressure minimum remains between 980 and 1000 hPa during the following 18 hours, while the low-pressure system moves northward along the coast.

4. Forecast performance

Verification focuses on mean-sea-level-pressure (MSLP), total precipitation (defined as the sum of rainfall and snowfall) and snowfall at key times. MSLP forecasts are verified at 12 UTC of the 25th and the 26th and precipitation forecasts are verified against observed values accumulated between the 24th and the 25th and between the 25th and the 26th of January 2000. Snowfall is predicted directly by the ECMWF cloud scheme (*Tiedke* 1989, 1993). Snowfall is verified for six stations archived in the ECMWF database that reported snow depth at 12 UTC on the 24th, 25th and 26th of January (Bagotville, Quebec; Robertval, Quebec; New York La Guardia; Baltimore-Washington International; Rochester NY; Raleigh, North Carolina; see Table 1). Snowfall forecast values have been interpolated from the four closest grid-points. Both snowfall and total precipitation are reported in mm of equivalent water (1mm of snowfall is equivalent to approximately 1cm of fresh snow over ground).

4.1 Verification measures

The accuracy of deterministic forecasts of MSLP is assessed by computing root-mean-square error (RMSE), intensity, position and 24h-tendency errors (IE, PE, TE). Root-mean-square errors are computed inside a box of 30° in latitude and 40° in longitude centered on the cyclone position at the verification time. Intensity and position errors are computed by comparing the observed cyclone intensity and position with the forecast relative minimum inside a 1200km radius from the observed cyclone (the software that identifies the cyclone position was kindly provided by Martin Leutbecher). Tendency errors are computed by comparing the observed and the forecast change in MSLP at the center of the storm over a 24h forecast period. RMSE is a simple and widely used measure to assess forecast accuracy. RMSE is sensitive to errors in gradient or intensity, so slight displacements of features characterized by strong gradients can lead to large RMSEs even if forecasts are qualitatively good. More sophisticated objective measures, in which errors are partitioned into misplacement and shape errors (*Hoffman et al.* 1995, *Douglas* 1997) are still under development and are not commonly used in operational environments. The combined use of RMSE, IE, PE and TE is contrasted with a subjective verification. This approach should give a comprehensive overview of MSLP forecast accuracy. Precipitation and snowfall predictions are assessed subjectively by comparing observed and predicted fields.

4.2 Performance of the T_L319 and the EPS control forecasts

Figure 3 shows the root-mean-square, intensity and position errors of the T_L319 and the EPS control MSLP forecasts with initial conditions from the 18th (t+168h forecast) to the 24th (t+24h) of January and verified at 12UTC of the 25th. The two forecasts have very similar root-mean-square and intensity errors (Figs. 3a,b), while the higher-resolution T_L319 forecast has lower position errors (Fig. 3c) for all lead times apart for 24 hours. Intensity errors are larger than 5hPa for forecasts with a 48-hour or a longer lead-time (Fig. 3b), and position errors are 200km or larger for all forecast times (Fig. 3c). Table 2 lists the MSLP tendency errors in predicting the observed 23hPa/d pressure fall for forecasts with a lead-time of 96 hours or less. Table 2 shows that the T_L319 have a TE larger than 9hPa/d for lead times of 48 hours or longer (the TE of the EPS control forecast is similar to the TE of the T_L319 forecast, not shown).

Figure 4 shows the errors of the ECMWF T_L319 and the EPS control MSLP forecasts verified on the 26th (12 UTC). The T_L319 and the EPS control forecasts have similar root-mean-square and intensity errors (Fig. 4a,b) while the T_L319 forecast has lower position errors (Fig. 4c). Compared to the forecasts with the same lead-time verified on the 25th (Fig. 3b), forecasts verified on the 26th (Fig. 4b) have smaller intensity errors. The situation at the surface is easier to predict than the day before: the storm central pressure at 12 UTC of the 26th is higher than the day before (991.1hPa compared to 984.4hPa) and the 24h-variation in the pressure minimum is a factor of 3 smaller. Table 2 shows that also the TE of the ECMWF T_L319 and the EPS control forecasts verified on the 26th are smaller than the TE of the forecasts valid for the 25th.

Figures 5-to-8 show the observed and predicted flow at the surface. The first row of Figure 5 shows the verifying analysis at 12 UTC on the 25th of January and the t+72h MSLP forecasts given by the T_L319 and the EPS control issued on the 22nd. Both forecasts predict a rather large area of low pressure with a smooth pressure gradient, with minimum values northeast of the observed minimum. The first row of Fig. 6 shows the corresponding t+48h forecasts produced the day after and still valid for 12 UTC of the 25th. The 48-h forecasts (Fig. 6b,c) predict a more localized area of low pressure than the 72-h forecasts, but they still position the pressure minimum too far off the East Coast and fail to correctly intensify the cyclonic system (Table 2).

The first row of Figs. 7 and 8 show the verifying analysis valid for 12 UTC on the 26th of January and the t+72h and the t+48h MSLP forecasts given by the T_L319 and the EPS control. As it is the case of the forecasts valid for 12 UTC of the 25th, the t+72h forecasts valid for the 26th (Fig. 7b,c) fail to predict the location of the area of low pressure and its associated pressure gradient. The 48-h forecasts (Fig. 8b,c) predict almost correctly the position but over intensify the cyclonic development.

Figure 9 shows the T_L319 24h-accumulated forecasts of precipitation (left) and snowfall (right) issued on the 24th (t+24h), the 23rd (t+48h) and the 22nd (t+72h) and valid for the 25th. (Since the t+72h and the t+48h EPS control forecasts are very similar to the T_L319 forecast, only the latter are shown.) Over land, the t+24h T_L319 precipitation forecast (Fig. 9a, see Fig. 1a for observations) predicts the area of precipitation almost correctly, with a small misplacement of the area of intense precipitation (40mm) around 3°4N degrees of latitude and with no indication of observed precipitation north of 40°N degrees (Philadelphia and New York area). Figures 9a,b show that over northeastern US precipitation is mostly predicted as snowfall, with no snowfall predicted south of 32°N degrees (Georgia, Florida). The t+48h T_L319 forecasts (Fig. 9c,d) are less accurate than the 24-h forecasts, with the band of precipitation predicted too little inland and with no indication of more than 10mm of precipitation around 34°N degrees (the Carolinas). The t+72h forecasts (Fig. 9e,f) are less accurate, with only 1-5 mm of rainfall predicted over land. The first three columns of Table 1 lists the observed snowfall and the T_L319 48-h and 72-h predictions at the six selected stations. Results are in agreement with the synoptic evaluation, and confirm that deterministic predictions underestimate the observed snowfall at NY La Guardia, Baltimore-Washington International and Bagotville and overestimate snowfall at Robertval and Rochester.

Figure 10 shows the T_L319 24h-accumulated forecasts of precipitation (left) and snowfall (right) issued on the 25th (t+24h), the 24th (t+48h) and the 23rd (t+72h) and valid for the 26th. Over land, the t+24h T_L319 precipitation forecast (Fig. 10a) fails to predict the area of more than 20mm precipitation (Fig. 1b) around

40-42°N degrees (New York, Boston area). The comparison between the maps of forecast precipitation and snowfall (Fig. 10a,b) indicates that almost all precipitation is predicted as snowfall, in agreement with the observed thermal structure (Fig. 1f). The t+48h T_L319 forecast (Fig. 10c) keeps the band of precipitation too much toward the coast and fails to produce more than 10mm of precipitation. The comparison between the t+48h precipitation and snowfall predictions indicates again that almost all precipitation is predicted as snowfall. The t+72h forecast (Fig. 10e) fails to predict any precipitation over land where it is observed (Fig. 1b). The last three columns of Table 1 lists the observed snowfall and the T_L319 48-h and 72-h predictions at the six selected stations. Results indicate a general underestimation of snowfall apart for the 72-h forecast for New York La Guardia.

4.3 Performance of the ECMWF EPS

First, the EPS performance in predicting MSLP is assessed by considering the number of EPS members with intensity and position errors smaller than 5hPa/200km, 10hPa/400km and 15hPa/600km. Figure 3d shows this diagnostic for the EPS forecasts with initial conditions from the 18th (t+168h forecast) to the 24th (t+24h) and valid for the 25th of January (12 UTC). Results indicate that for lead times of 120-h or longer no EPS members predict the storm with IE/PE smaller than 10hPa/400km, and that two EPS members predict the storm with such an accuracy for 96- and 72-hour lead times. This number increases substantially (from two to fifteen) in the following 24 hours. Then the EPS performance is assessed in terms of tendency errors. Table 2 shows that on the 21st (t+96h) nine EPS members predict that storm intensification with a TE smaller than 5hPa/d (five members with TE smaller than 2.5hPa/d). On the 22nd (t+72h), three EPS members predict the storm intensification with a TE of less than 5hP/da and eleven members predict the storm with a TE smaller than 10hPa/d.

Figures 5 and 6 show (second and third row) the MSLP forecasts given by the ensemble-mean and by five EPS members started on the 22nd (+72h) and the 23rd (+48h) of January. The five EPS members are chosen to include the two members with the smallest RMSE and the three members with the smallest IE. Figure 5 shows that members 25, 50 and 11 (last row) predict the storm with, respectively IE/PE of 1hPa/1065km, 4.9hPa/425km and 5hPa/169km. By contrast, the T_L319 and the EPS control forecasts (Fig. 5, top row) have IE/PE of, respectively, 19.3hPa/400km and 19.3hPa/609km. In RMSE terms, ten EPS members have an error smaller than the T_L319 and eighteen members have an error smaller than the EPS control. Figure 6 shows that the 48-hour forecasts are more accurate, with four EPS members with IE less than 0.3hPa (members 3, 9, 40 and 41, see middle and bottom rows of Fig. 6), among which is one (member 3) with a 78km PE. By contrast, both the T_L319 and the EPS control forecasts have IE/PE larger than 9.4hPa/564km (see top row of Fig. 6). For both forecast steps, the ensemble-mean forecast (first panel of the second row in Figs. 5 and 6) is too smooth a field to be used to predict such an extreme event associated with a strong pressure gradient.

Figure 4d shows the number of EPS members with intensity and position errors smaller than 5hPa/200km, 10hPa/400km and 15hPa/600km for the forecasts with initial conditions from the 19th (t+168h forecast) to the 25th (t+24h) and valid for the 26th of January (12 UTC). Results show that for any lead-time at least one EPS member has IE/PE smaller than 10hPa/400km, and that this number increases as the lead-time decreases. Considering IE/PE smaller than 5Pa/200km, Fig. 4d shows that two or more members have such accuracy only for lead-times of 72 hours or less. Table 2 shows that forecasts valid for 12 UTC of the 26th

more accurately predict also the storm intensification, with more than nine members with a TE smaller than 2.5hPa/d for lead times of 96 hours or shorter.

Figures 7 and 8 show the MSLP forecasts given by the ensemble-mean and by five EPS members (selected as discussed above) started on the 23rd (+72h) and the 24th (+48h) of January and valid for 12GMT of the 26th. Figure 7 (last row) shows that EPS members 22, 47 and 7 predict the storm with, respectively, IE/PE of 3.2hPa/518km, 3.2hPa/189km and 3.7hPa/494km. By contrast, the T_L319 and the EPS control forecasts (Fig. 7, top row) have IE/PE of, respectively, 13hPa/541km and 20.1hPa/770km. In RMSE terms, twenty-seven EPS members have an error smaller than the T_L319 and thirty members had an error smaller than the EPS control. Figure 8 shows that 48-hour forecasts are more accurate, with three EPS members with IE less than 0.8hPa (members 13, 48 and 50, see middle and bottom rows of Fig. 7), among which one (member 13) with a 56km PE. By contrast, both the T_L319 and EPS control forecasts have IE larger than 6hPa (see top row of Fig. 8). For the 72-hour forecast range, the ensemble-mean forecast (first panel of the second row in Figs. 7) proves again to be too smooth a field to be used to predict extreme events, while the 48-hour ensemble-mean (Fig. 8) predicts the observed cyclone with a high degree of accuracy. This is due to the fact that a large number of 48-h perturbed forecasts have very low intensity and position errors (Fig. 4d).

Consider now precipitation and snowfall forecasts. Attention is focused on lead-times up to 72 hours and predictions of probabilities of 24-h accumulated precipitation or snowfall exceeding predefined thresholds. Figure 11 shows the probability of "24-h precipitation in excess of 10mm" (left) and "24-h accumulated snowfall in excess of 10mm" (right) predicted on the 24th (t+24h), the 23rd (t+48h) and the 22nd (t+72h) and valid for the 24-h ending at 12 UTC of the 25th. Precipitation predictions can be compared over land with the observed field (Fig. 1a,b). Figure 11 shows that the t+24h forecast issued on the 24th gives a 60% probability of precipitation in excess of 10mm over the area where 10mm is observed (see Fig. 1a). The t+72h forecast issued on the 22nd gives a 2-to-10% probability of precipitation in excess of 10mm (Fig. 11e) over the area where 10mm is observed. The 48-h EPS indicates a 10-30% probability of precipitation in excess of 10mm (Fig. 11c) over the East Coast where 10mm of precipitation is observed (Fig. 1a), with a 30-60% probability over North Carolina (about 36°N degrees). Forecast probabilities are even higher in the 24-h forecast (Fig. 11a). Similarly, the probabilities of snowfall in excess of 10mm increases from zero in the t+72h forecast (Fig. 11f), to 2-to-10% in the t+48h forecast (Fig. 11d) and up to 30% in the t+24h forecast (Fig. 11b). Figure 12 is the equivalent of Fig. 11 but for a 20mm threshold. For this higher threshold the probability of precipitation are only slightly smaller than for 10mm and cover a slightly smaller area over land, but snowfall probabilities are about a factor of 3-to-5 smaller. In particular, the t+48h forecast gives a 10% probability of snowfall in excess of 20mm only between 34° and 36°N degrees (the Carolinas). Consistent signals can be detected in the EPS forecasts started on consecutive days, with probabilities increasing from small to large values as the verification time approaches.

The fact that, for equivalent thresholds, snowfall probabilities are lower than precipitation probabilities is a consequence of the fact that each EPS member has a different thermal structure. Figure 13 shows the observed position of the 0°C isotherm for 2m-temperature and its position in the 72-h, 48-h and 24-h forecasts valid for the 25th (left and the 26th (right). Figure 13 shows that for the forecasts valid for the 25th

the observed position of the 0°C isotherm is close to the edge of the range spanned by the EPS, especially in the 48-h and the 72-h forecasts.

Figure 14 shows the probability of "24-h precipitation in excess of 10mm" (left) and "24-h accumulated snowfall in excess of 10mm" (right) predicted on the 25th (t+24h), the 24th (t+48h) and the 23rd (t+72h) and valid for the 24-h ending at 12 UTC of the 26th. Precipitation predictions can be compared over land with the observed field (Fig. 1b). Figure 14a shows that the 24-h EPS issued on the 25th gives a 60% or higher probability of precipitation in excess of 10mm in a coastal region north of 36°N, in agreement with the observed field (Fig. 1c), but fails to predict the possibility of more than 10mm of precipitation in a very small region centered at 35°N, 78°W (Raleigh, North Carolina). The 24-h EPS gives a 10-to-30% probability of snowfall in excess of 10mm for a smaller region north of 38°N (Fig. 14b) where more than 10mm of snowfall is observed (Fig. 1d). The 48-h EPS probability forecasts issued on the 24th for both precipitation and snowfall in excess of 10mm (Figs. 14c,d) cover a larger area and have lower probability values than the 24th probability forecasts. The 72-h EPS probability maps cover a small area over the northeast coast and give a 2-to-10% probability of precipitation and snowfall in excess of 10mm. The right panels of Fig. 13 show the observed and forecast positions of the 0°C isotherm for 2m-temperature. Figure 13 shows that almost all EPS members predict the position the 0°C isotherm for 2m-temperature too much inland compared to the observed position, which lies close to the southeastern edge of the distribution of 0°C-isotherm forecast positions. Forecast probability maps of precipitation and snowfall in excess of 20mm cover a much smaller area and have smaller values (not shown), qualitatively in agreement to the fact that 20mm are observed only over a small region centered at 44°N (Massachusetts, New Hampshire).

Table 3 lists the EPS snowfall predictions at the six selected stations. Note that, for all stations, the observed value lies inside the EPS predicted range almost for all forecasts. The only large difference can be detected in the 72-h forecast for Baltimore-Washington International (Table 3d, 28mm observed and 22.8mm maximum prediction).

4.4 Summary of deterministic and probabilistic prediction

4.4.1 Verification time: 12UTC of the 25th - Deterministic predictions:

- The 72-h MSLP (Figs. 3 and 5, Table 2) and precipitation (Fig. 9, Table 2) forecasts fail.
- The 48-h MSLP forecasts fail to predict the storm position and rapid intensification (Figs. 3 and 6, Table 2); precipitation and snowfall predictions give some indications of coastal impact but keep the predicted area too little inland and underestimate the precipitation amount by about a factor of 2 (Fig. 9, Table 1).
- The 24-h MSLP T_L319 and the EPS control forecasts predict the storm (200 and 360km PE, respectively, and about 2 hPa IE; Fig. 3, Table 2); precipitation and snowfall predictions are reasonably accurate in position and amount (Fig. 9, Table 1).

4.4.2 Verification time 12UTC of the 25th - Probabilistic predictions:

- The 72-h MSLP prediction (Figs. 3d and 5, Table 2) gives some indication of a storm approaching the east coast (2 members with IE<10hPa, PE<400km, TE<5hPa/d); the 72-h prediction gives a 2-to-10% probability of precipitation and snowfall in excess of 10mm (Figs. 11 and 12, Table 3).

- The 48-h MSLP prediction has several members with a very accurate prediction of the storm position and rapid intensification (5 members with IE<5hPa, PE<200km and TE<2.5hPa/d; 16 members with IE<10hPa, PE<400km and TE<5hPa/d; see Figs. 3d and 6, Table 2); the 48-h prediction gives a 10-60% (2-30%) probabilities of precipitation and snowfall in excess of 10mm (20mm) over the East Coast where this amount of precipitation is observed (Figs. 11 and 12, Table 3).

- The 24-h MSLP prediction has 14 members with IE/PE smaller than 5hPa/200km (Fig. 3d); the 24-h prediction gives a 60-100% (30-100%) probability of precipitation in excess of 10mm (20mm) in the region where this is observed (Fig. 11 and 12).

4.4.3 Verification time 12UTC of the 26th - Deterministic predictions:

- 72-h MSLP (Figs. 4 and 7, Table 2) and precipitation (Fig. 10, Table 1) forecasts fail;

- 48-h MSLP T_L319 and the EPS control forecasts predict the storm position with a PE of about 200km, an IE of 6 and 8 hPa, respectively, and a TE of about 3hPa/d (Figs. 4 and 8, Table 2); precipitation and snowfall predictions almost correctly identify the area but underestimate the largest amounts by about a factor of 2 (Fig. 10, Table 1);

- 24-h MSLP T_L319 and the EPS control forecasts predict the storm with a very small PE and slightly over-intensify the minimum pressure (IE of about 2 hPa IE; Fig. 4); precipitation and snowfall predictions are rather accurate in position and amount (Fig. 10, Table 1).

4.4.4 Verification time 12UTC of the 26th - Probabilistic predictions:

- 72-h MSLP prediction (Figs. 4d and 7, Table 2) gives some accurate predictions of the storm moving northward along the east coast (2 members with IE<5hPa, PE<200km, TE<2.5hPa/d; 7 members with IE<10hPa, PE<400km, TE<5hPa/d); 72-h prediction gives a 2-10% probability of precipitation/snowfall (Fig. 14, Table 3);

- 48-h MSLP prediction has many members with a very accurate prediction of the storm position and rapid intensification (8 members with IE<5hPa, PE<200km and TE<2.5hPa/d; 21 members with IE<10hPa, PE<400km and TE<5hPa/d; see Figs. 4d and 8, Table 2); 48-h prediction gives a 30-60% probability of precipitation and snowfall in excess of 10mm over the East Coast where more than 10mm of precipitation is observed (Fig. 14, Table 3);

- 24-h MSLP predictions are very accurate (20 members have IE<2.5hPa, PE<200km and TE<2.5hPa/d; see Fig. 4d and Table 2); precipitation and snowfall predictions are very accurate in position and amount (Fig. 14).

5. Role of initial perturbations and of stochastic physics

A second set of ensemble experiments has been performed to investigate the influence of stochastic perturbations added to the tendencies due to parameterized physical processes (*Buizza et al.* 1999a). The results of this sensitivity analysis should be considered as a documentation of the relative impact of stochastic perturbations compared to the initial perturbations. The reader is referred to published literature (e.g. *Buizza et al.* 1999, *Mullen & Buizza* 2001) for more complete sensitivity studies based on larger sets of cases. These experiments can also give some indications on the sensitivity of forecast errors to moist processes during this case.

This second set of ensembles (NOST) has been run at the same resolution as the operational ensemble but without stochastic perturbations for starting dates from the 19th to the 25th of January. Considering MSLP predictions, Fig. 15 shows the number of ensemble members with intensity and position errors smaller than 5hPa/200km, 10hPa/400km and 15hPa/400km for the NOST and the operational EPS (run with stochastic physics). The ensembles run without the stochastic forcing have a smaller number of members with small IE/PE for all lead-times apart for the 48-hour forecasts started on the 24th and verified on the 26th of January (Fig. 15b). Results indicate that the NOST ensembles are less able to correctly intensify the cyclone especially for forecast times longer than 48 hours.

An example of the positive impact of stochastic physics is given by the comparison of the +72h forecast started on the 23rd and valid for the 26th. Figure 16 shows selected NOST ensemble members to be compared with the selected EPS members shown in Fig. 7. It is interesting to note that member number 18 and member number 2 are the RMSE-best members for both types of ensembles, and that stochastic physics reduces the RMSE of one of them and the IE for both forecasts. The comparison of the three NOST and EPS members with the smallest IE suggests that the cyclone intensity and position is more accurate in the EPS (run with stochastic physics) than in the NOST ensemble forecasts.

Precipitation and snowfall predictions given by the NOST ensemble have been compared with the respective predictions given by the operational EPS. Little differences can be identified between the NOST-ensemble (not shown) and the EPS 48-h probability maps for the events ‘precipitation/snowfall larger than 10mm and 20mm’. The difference is more evident in the 72-h forecasts: over the East Coast, the EPS probabilities extend more inland than the NOST probabilities (not shown), in better agreement with the observations. In Table 4 the average (among the six selected stations) observed value is contrasted with the EPS and the NOST-ensemble median, 75th and 95th percentiles and maximum predicted values. Results indicate that the EPS predicted values are about 10% larger than the NOST values.

Three 72-h forecasts valid for 12 UTC on the 26th of January are compared to document in more details the impact of initial perturbations and stochastic physics. The selected forecasts are the EPS control forecast (CON), the EPS member 2 (EPS2), which is the EPS member with the second lowest RMSE and the third lowest IE (see Fig. 7f), and member 2 run without stochastic physics (NOST2, see Fig. 16f). Figures 7 and 16 show that EPS2 has a lower RMSE, a lower IE but a larger PE than NOST2 (RMSE: 3.4hPa versus 4.1hPa; IE: 3.4hPa versus 9.6hP; PE: 558km versus 183km). The 72-h control forecast shows two weak

minima (Fig. 7c), both wrongly located, one at about (55N, 40W) and one at about (40N, 65W). By contrast, EPS2 shows (Fig. 7f) a unique, more correctly positioned minimum.

Figure 17 shows the differences (EPS2-CON), (NOST2-CON) and (EPS2-NOST2) and the errors of the three forecasts in terms of MSLP. The left panels of Fig. 17 show that (EPS2-CON) and (NOST2-CON) are rather similar, and that (EPS2-NOST2) is smaller than (EPS2-CON) and (NOST2-CON). This indicates that stochastic physics has a smaller impact than the initial perturbation added to generate the perturbed initial condition of EPS member number 2. Figure 17e shows that stochastic physics intensifies the cyclone in the 72-h forecast. The comparison of the error fields (Fig. 17, right panels) shows that both EPS2 and NOST2 have smaller errors than the control. The analysis of the evolution of (EPS2-CON) with forecast time (not shown) indicate that the difference at t+72-h starts at t+24h over northern Florida (at about 30N, 80W) and propagates north-eastward along the coast line.

Figure 18 is analogous to Fig. 17 but shows a vertical cross section (longitude versus pressure) of temperature differences averaged in latitude between 30ºN and 60ºN degrees latitude. The left panels of Fig. 18 confirm that stochastic physics has a smaller impact than the initial perturbation and that both EPS2 and NOST2 have smaller errors than the control forecast. Stochastic physics induces some cooling in the lower troposphere around 70ºW degree longitude (Fig. 18a,c) in correspondence of the difference in MSLP (Fig. 17a,c). The initial perturbation added to member 2 induces a warming of the whole air column in correspondence with the cyclone evolution (Fig. 18c), and this reduces substantially the temperature errors (Fig. 18, right panels).

Figure 19 is analogous to Figs. 17 and 18 but shows differences between 24-h accumulated precipitation predictions valid for the 26th of January. Figure 19 shows that EPS2 and NOST2 have both more intense precipitation over land than the control forecast, and that stochastic physics induces a shift of the precipitation band over sea but has a very small effect over land.

6. Conclusion

Explosive cyclogenesis over the East Coast of United States is a relatively rare event (*Kocin & Uccellini* 1990) that is still rather difficult to predict, with skillful prediction alternated with forecast failures (*Mullen & Baumhefner* 1994). One of these severe winter weather events affected the US East Coast between the 24th and the 26th of January 2000, when MSLP drop about 23hPa between 12UTC of the 24th and the 25th and snowfall between the 25th and the 26th paralyzed part of the US East Coast. The performance of the ECMWF T_L319L60 high-resolution model and of the T_L159L40 Ensemble Prediction System during the US storm of the 25th and the 26th of January 2000 has been discussed. Attention has been focused on mean-sea-level-pressure (MSLP), snowfall and total precipitation prediction.

The most critical period to predict coincided with the rapid development of the storm between the 24th and the 25th of January. For this period, single (T_L319 and EPS control) deterministic forecasts issued 48-h and 72-h before the event failed to intensify the storm, wrongly predicted the area affected by precipitation over land and underestimated the overall amount of precipitation by about a factor of 2. Shorter, 24-h deterministic forecasts also failed to correctly predict the storm position and intensification, but at least gave

a more accurate precipitation prediction. By contrast, 72-h EPS forecast gave some indication of the possibility of the storm developments and predicted a 2-to-10% probability of precipitation and snowfall in excess of 10mm in a region where 10mm values were observed. The 48-h EPS forecasts were more accurate, with 16 members predicting the storm with intensity error IE<10hPa, position error PE<400km and tendency error TE<5hPa/d. The 48-h EPS prediction gave a 10-to-60% probability of precipitation and snowfall in excess of 10mm and a 2-to-30% probability of values in excess of 20mm for regions where these amounts were observed. The 24-h EPS predictions had 14 members with intensity/position errors IE<5hPa and PE<200km and gave high probabilities of precipitation and snowfall in excess of 10 and 20mm in the area where these amounts were observed. Both deterministic and probabilistic predictions of the storm development during the following 24 hours, between the 25th and the 26th of January, were more accurate.

The comparison of the (T_L319 and EPS control) single deterministic and the EPS probabilistic forecasts indicates that the EPS gave some indications of the developments of the storm 24 to 48 hours before single deterministic forecasts. The consistency of EPS forecasts issued on consecutive days made ensemble probabilistic forecasts particularly useful.

One of the key issues to be addressed when promoting the use of ensemble forecast products is how forecasters should use ensemble-generated products to assess the risk of severe weather disruption. Despite the fact that guidelines can only be drawn after a statistical analysis of a large sample of cases, this work gives some indications of possible ensemble products. Results suggest that for this type of severe winter weather events EPS probability maps of precipitation and snowfall, maps showing the position of the 0°C isoline of the 2m temperature field combined with synoptic charts of MSLP of all ensemble members can be used to assess the severity of a forecast situation. Results also indicate that the ensemble-mean field is too smooth a field to be used to predict severe weather events associated with a strong pressure gradient.

Confidence in the quality of the EPS can be consolidated only through statistical analyses of the performance over long periods (*Talagrand et al.* 1999). The reader is referred to published literature (*Buizza et al.* 1999b, *Barkmeijer et al.* 2001, *Mullen & Buizza* 2001, *Buizza & Hollingsworth* 2002) for more detailed analysis of the performance of the EPS during longer periods.

Results from sensitivity experiments have shown that stochastic physics has in general a smaller impact than initial perturbations on the EPS perturbed forecasts and that the combination of initial perturbations and stochastic physics improves the quality of the EPS performance. These results confirm the positive impact of the stochastic scheme on the EPS performance reported in *Buizza et al.* (1999a) and *Mullen & Buizza* (2001). In particular, the results from this sensitivity analysis suggest that forecast errors in the prediction of the 24-26 January US Storm were very sensitive to moist processes.

Acknowledgements

The authors would like to thank Martin Leutbecher, who developed a first version of the code to identify MSLP minimum values and Steve Mullen for providing observed precipitation data for the US-storm case study. Anders Persson, Tony Hollingsworth and Tim Palmer are acknowledged for their useful comments to an early version of this manuscript. The authors would also like to thank the editor Dr D. P. Jorgensen and

three anonymous reviewers whose comments and suggestions helped improving the quality of the manuscript.

References

Barkmeijer, J., Buizza, R., & Palmer, T. N., 1999: 3D-Var Hessian singular vectors and their potential use in the ECMWF Ensemble Prediction System. *Q. J. R. Meteor. Soc.*, **125**, 2333-2351.

————, Buizza, R., Palmer, T. N., Puri, K., & Mahfouf, J.-F., 2001: Tropical singular vectors computed with linearized diabatic physics. *Q. J. R. Meteorol. Soc.*, **127**, 685-708.

Buizza, R., & Hollingsworth, A., 2002: Storm prediction over Europe using the ECMWF Ensemble Prediction System. *Meteorol. Appl.*, in press. Also published as *ECMWF Tech. Memo*. No.356.

————, Petroliagis, T., Palmer, T. N., Barkmeijer, J., Hamrud, M., Hollingsworth, A., Simmons, A., & Wedi, N., 1998: Impact of model resolution and ensemble size on the performance of the ECMWF ensemble prediction system. *Q. J. R. Meteorol. Soc.*, **124**, 1935-1960.

————, Miller, M., & Palmer, T. N., 1999a: Stochastic representation of model uncertainties in the ECMWF Ensemble Prediction System. *Q. J. R. Meteorol. Soc.*, **125**, 2887-2908.

————, Barkmeijer, J, Palmer, T N, & Richardson, D, 1999b. Current Status and Future Developments of the ECMWF Ensemble Prediction System. *Meteorol. Appl.*, 6, 1-14.

————, Hollingsworth, A., Lalaurette, F., & Ghelli, A., 1999c: Probabilistic predictions of precipitation using the ECMWF Ensemble Prediction System. *Weather and Forecasting*, **14**., 2, 168-189

————, Hollingsworth, A., Lalaurette, F., & Ghelli, A., 2000: Reply to comments by Dr L. J. Wilson. *Weather and Forecasting*, **15**, 367-369.

Carlson, T. N., 1991: *Mid-Latitude Weather Systems,* Harper Collins Academic, London, 507 pp.

Douglas, R., J., 1997:*Decomposition of weather forecast error using rearrangements of functions*, Met. Office Forecasting Research, Tech, Rep. No.216

Easterling, D. R., Evans, J. L., Groisman, P. Ya., Karl, T. R., Kunkel, K. E., & Ambenje, P., 1999: Observed variability and trends in severe weather climate events: a brief reviw. *Bull. Amer. Meteorol. Soc.*, **81**, 417-425.

Ehrendorfer, M., 1994a: The Liouville equation and its potential usefulness for the prediction of forecast skill. Part I: theory. *Mon. Wea. Rev.* **122**, 703-713.

————, Tribbia, J., & Errico, R. M., 1995: Mesoscale predictability: an assessment trhoygh adjoint methods. *Proceedings of the ECMWF Seminar on Predictability, 4-8 September 1995, Vol I*, ECMWF, Shinfield Park, Reading RG2 9AX, UK, 157-183.

————, 1994b: The Liouville equation and its potential usefulness for the prediction of forecast skill. Part II: applications. *Mon. Wea. Rev.* **122**, 714-728.

Epstein, E. S., 1969: A scoring system for probability forecasts of ranked categories. *J. Appl. Meteorol.*, **8**, 985-987.

Gleeson, T. A., 1966: A causal relation for probabilities in synoptic meteorology. *J. Appl. Meteorol.*, **5**, 365-8.

Hoffman, R. N., Liu, Z. Louis, J.F. and Grassotti, C.1995: *Distortion representation of forecast erors,* Mon. Wea. Rev. **123**, 2758-2770

Houtekamer, P. L., Lefaivre, L., Derome, J., Ritchie, H., & Mitchell, H. L., 1996: A system simulation approach to ensemble prediction. *Mon. Wea. Rev.*, **124**, 1225-1242.

Kocin, P. J. and Uccellini L. W., 1990: *Snowstorms Along the Northeastern Coast of the United States: 1955 to 1985,* American Meteorlogical Society, pp. 280 (ISBN0-933876-90-4)

Kunkel, K. E., Pielke Jr., R. A., & Changnon, S. A., 1999: Temporal fluctuations in weather and climate extremes that cause economic and human health impacts: A review. *Bull. Amer. Meteorol. Soc.*, **80**, 1077-1098.

Lorenz, E. N., 1969: The predictability of a flow which possesses many scales of motion. *Tellus*, **34**, 505-513.

Manobianco, M., 1989: Explosive East Coast Cyclogenesis over the West-Central North Atlantic Ocean: A composite Study Derived from ECMWF Operational Analyses. *Mon. Wea. Rev,* **117,** 2365- 2583.

Molteni, F., Buizza, R., Palmer, T. N., & Petroliagis, T., 1996: The ECMWF Ensemble Prediction System: methodology and validation. *Q. J. R. Meteorol. Soc.*, **122**, 73-119.

Mullen, S. T., & Baumhefner, D., P., 1994: Monte Carlo Simulations of Explosive Cyclogenesis. *Mon. Wea. Rev,* **122,** 1548-1567.

————, & Buizza, R., 2001: Quantitative precipitation forecasts over the United States by the ECMWF Ensemble Prediction System. *Mon. Wea. Rev.*,**129**, 638-663.

Palmer, T. N., 2000: Predicting uncertainty in forecasts of weather and climate. *Rep. Prog. Phys.*, **63**, 71-116.

————, Molteni, F., Mureau, R., Buizza, R., Chapelet, P, & Tribbia, J., 1993: Ensemble Prediction. *Proc. ECMWF Seminar (1992)*, ECMWF, Shinfield Park, Reading RG2-9AX, UK.

Petroliagis, T., Buizza, R., Lanzinger, A., & Palmer, T. N., 1997: Potential use of the ECMWF Ensemble Prediction System in cases of extreme weather events. *Meteorol. Appl.*, **4**, 69-84

Sanders, F., & Gyakum, J. R., 1980: Synoptic-dynamic climatology of the "Bomb". *Mon. Wea. Rev.*, **108**, 1589-1606.

Talagrand, O., Vautard, R., & Strauss, B., 1999: Evaluation of probabilistic prediction systems. *Proceedings of the ECMWF Workshop on Predictability*, ECMWF, Reading, 20-22 October 1997, 1-26.

Teixeira, J., 1999: The impact of increased boundary layer vertical resolution on the ECMWF forecast system. *ECMWF Research department Technical Memorandum No. 268*, ECMWF, Shinfield Park, Reading RG2 9AX, UK, 55pp.

Tiedke, M., 1989: A comprehensive mass flux scheme for cumulus parametrisation in large-scale models. *Mon. Wea. Rev.* **117**, 1779-1800.

————, 1993: Representation of clouds in large-scale models. *Mon. Wea. Rev.* **121**, 3040-3061.

Toth, Z., & Kalnay, E., 1993: Ensemble forecasting at NMC: the generation of perturbations. *Bull. Am. Meteorol. Soc.*, **74**, 2317-2330.

————, 1997: Ensemble forecasting at NCEP and the breeding method. *Mon. Wea. Rev.*, **125**, 3297-3319.

Tracton, M. S., & Kalnay, E., 1993: Operational ensemble prediction at the National Meteorological Center: practical aspects. *Weather & Forecasting*, **8**, 379-398.

Station	Coord	SF (mm) acc. between 12 UTC of 24 to 25 Jan				SF (mm) acc. between 12 UTC of 25 to 26 Jan			
		Obs	+24h	+48h	+72h	Obs	+24h	+48h	+72h
Bagotville	**48.3N-71W**	1	0.6	0.4	1.3	9	7.3	0	3.0
Robertval	**48.5N-72.2W**	0	0.6	0.5	0.8	8	5.0	0.2	1.2
Rochester	**43.1N-77.6W**	0	0	0.1	0.8	10	3.6	0.3	0.8
NY LaG.	**40.7N-73.3W**	2	0.3	0.1	0.6	10	5.1	0	14.7
Ba.-Wash.	**39.1N-76.6W**	2	1.0	0.1	1.3	28	10.4	0	4.7
Raleigh	**35.8N-78.8W**	NN	8.4	0.8	0.7	8	2.4	0.2	3.0

Table 1. List of stations used to verify 24-h accumulated snowfall predictions by the TL319 operational model. The observed value for Raleigh is known only for the period from 12 UTC of the 25th to the 12UTC of the 26th. Snowfall is reported in mm of equivalent water (1mm of snowfall is equivalent to approximately 1cm of fresh snow over ground.

Initial date	Fc day d-1	Fc day d	Obs tendency	T_L319 TE	EPS # TE<5(2.5)	EPS # 5<TE<10	EPS # TE>10
21 Jan	+72h	+96h	23.1hPa/d	9.3hPa/d	9 (5)	11	29
22 Jan	+48h	+72h	23.1hPa/d	21.6hPa/d	3 (1)	8	40
23 Jan	+24h	+48h	23.1hPa/d	10.5hPa/d	16 (8)	10	24
22 Jan	+72h	+96h	6.7hPa/d	4.1hPa/d	27 (16)	15	9
23 Jan	+48h	+72h	6.7hPa/d	2.8hPa/d	21 (9)	15	13
24 Jan	+24h	+48h	6.7hPa/d	5.8hPa/d	37 (20)	14	0

Table 2. Observed and forecast 24-h change (tendency, hPa/d) in the minimum MSLP between 12UTC of the 24th and the 25th January (rows 1-3) and MSLP between 12UTC of the 25th and the 26th January (rows 4-6). The first 3 columns list the initial date and the two consecutive forecast steps, column 4 lists the observed change, column 5 lists the error TE in the TL319 tendency forecast, columns 6-8 lists the number of EPS members with TE smaller than 5hPa/d (TE smaller than 2.5hPa/d in brackets), with TE between 5 and 10hPa/d and with TE larger than 10hPa/d.

Bagotville (48.3N;71W)								
	Obs (mm)	**min**	**5 perc**	**25 perc**	**med**	**75 perc**	**95 perc**	**max**
24 Jan t+24h	1.0	0.4	0.5	0.5	0.6	0.7	0.8	0.8
23 Jan t+48h	1.0	0.2	0.2	0.3	0.4	0.6	1.0	4.0
22 Jan +72h	1.0	0.1	0.2	0.6	1.4	2.5	7.5	10.2
25 Jan t+24h	9.0	2.4	3.3	5.1	6.2	7.4	9.9	11.1
24 Jan +48h	9.0	0.1	0.1	1.4	2.9	5.2	8.2	9.4
22 Jan +72h	9.0	0.0	0.1	0.1	0.1	2.8	8.6	14.9

Table 3a. EPS t+24h, t+48h and t+72h snowfall forecasts for (a) Bagotville, (b) Robertval, (c) New York La Guardia, (d) Baltimore-Washington International Airport (e) Rochester and (f) Raleigh (24h accumulated values are expressed in mm of equivalent water). The observed value for Raleigh is known only for the period from 12 UTC of the 25th to the 12UTC of the 26th.

Robertval (48.5N;72.2W)								
	Obs (mm)	**min**	**5 perc**	**25 perc**	**med**	**75 perc**	**95 perc**	**max**
24 Jan t+24h	0.0	0.0	0.2	0.4	0.5	0.5	0.5	0.5
23 Jan t+48h	0.0	0.2	0.2	0.3	0.3	0.4	0.6	2.4
22 Jan +72h	0.0	0.1	0.2	0.5	0.8	1.4	4.3	5.5
25 Jan t+24h	8.0	1.1	2.0	3.1	4.3	5.4	7.3	8.1
24 Jan +48h	8.0	0.1	0.1	0.3	1.6	3.6	6.0	8.9
22 Jan +72h	8.0	0.0	0.1	0.1	0.2	0.8	7.1	9.2

Table 3b.

New York La Guardia (40.7N;73.3W)								
	Obs (mm)	**min**	**5 perc**	**25 perc**	**med**	**75 perc**	**95 perc**	**max**
24 Jan t+24h	2.0	0.0	0.0	0.0	0.3	1.4	5.0	7.3
23 Jan t+48h	2.0	0.0	0.0	0.0	1.0	3.4	14.8	25.1
22 Jan +72h	2.0	0.0	0.0	0.0	0.1	0.8	5.4	8.2
25 Jan t+24h	10.0	3.3	3.6	4.6	5.3	6.2	7.6	9.1
24 Jan +48h	10.0	0.0	2.6	6.3	9.8	12.9	16.3	19.2
22 Jan +72h	10.0	0.0	0.0	0.0	0.1	3.5	11.8	24.2

Table 3c.

Baltimore-Washington International (39.1N;76.6W)								
	Obs (mm)	min	5 perc	25 perc	med	75 perc	95 perc	max
24 Jan t+24h	2.0	0.0	0.0	0.2	1.9	4.1	11.0	20.0
23 Jan t+48h	2.0	0.0	0.0	0.0	0.6	2.7	13.9	34.4
22 Jan +72h	2.0	0.0	0.0	0.1	0.2	0.7	3.5	7.4
25 Jan t+24h	28.0	5.1	6.0	7.8	8.5	9.3	11.6	12.7
24 Jan +48h	28.0	0.0	0.2	6.3	10.4	15.2	20.0	29.1
22 Jan +72h	28.0	0.0	0.1	0.1	0.3	0.7	5.4	22.8

Table 3d.

Rochester (43.1N;77.6W)								
	Obs (mm)	min	5 perc	25 perc	med	75 perc	95 perc	max
24 Jan t+24h	0.0	0.0	0.0	0.1	0.1	0.2	0.3	0.3
23 Jan t+48h	0.0	0.1	0.1	0.1	0.2	0.2	0.6	7.2
22 Jan +72h	0.0	0.1	0.2	0.2	0.4	0.7	1.6	3.8
25 Jan t+24h	10.0	0.8	1.5	2.1	2.7	3.4	4.2	6.2
24 Jan +48h	10.0	0.2	0.4	0.5	1.4	4.9	11.7	16.4
22 Jan +72h	10.0	0.1	0.2	0.3	0.5	0.8	4.7	9.2

Table 3e.

Raleigh (35.8N;78.8W)								
	Obs (mm)	Min	5 perc	25 perc	med	75 perc	95 perc	max
24 Jan t+24h	Unknown	0.4	0.8	5.2	11.9	16.6	26.2	33.4
23 Jan t+48h	Unknown	0.0	0.0	0.0	0.2	2.4	12.9	31.9
22 Jan +72h	Unknown	0.0	0.0	0.0	0.0	0.1	1.3	3.3
25 Jan t+24h	8.0	2.1	2.2	2.5	2.7	2.8	3.2	3.3
24 Jan +48h	8.0	0.2	0.4	0.5	1.4	4.9	11.7	16.4
22 Jan +72h	8.0	0.1	0.2	0.3	0.5	0.8	4.7	9.2

Table 3f.

	Obs (mm)	EPS (Stochastic physics on)				NOST-ensemble			
		med	75prc	95prc	max	med	75prc	95prc	max
Ave	6.2	1.6	3.2	7.6	13.6	1.5	2.8	7.1	10.0

Table 4. 15-station average observed value (column 1) and average forecast statistics for the EPS (column 2-5) and for the NOST-ensemble (columns 6-9) (24h accumulated values are expressed in mm of equivalent water).

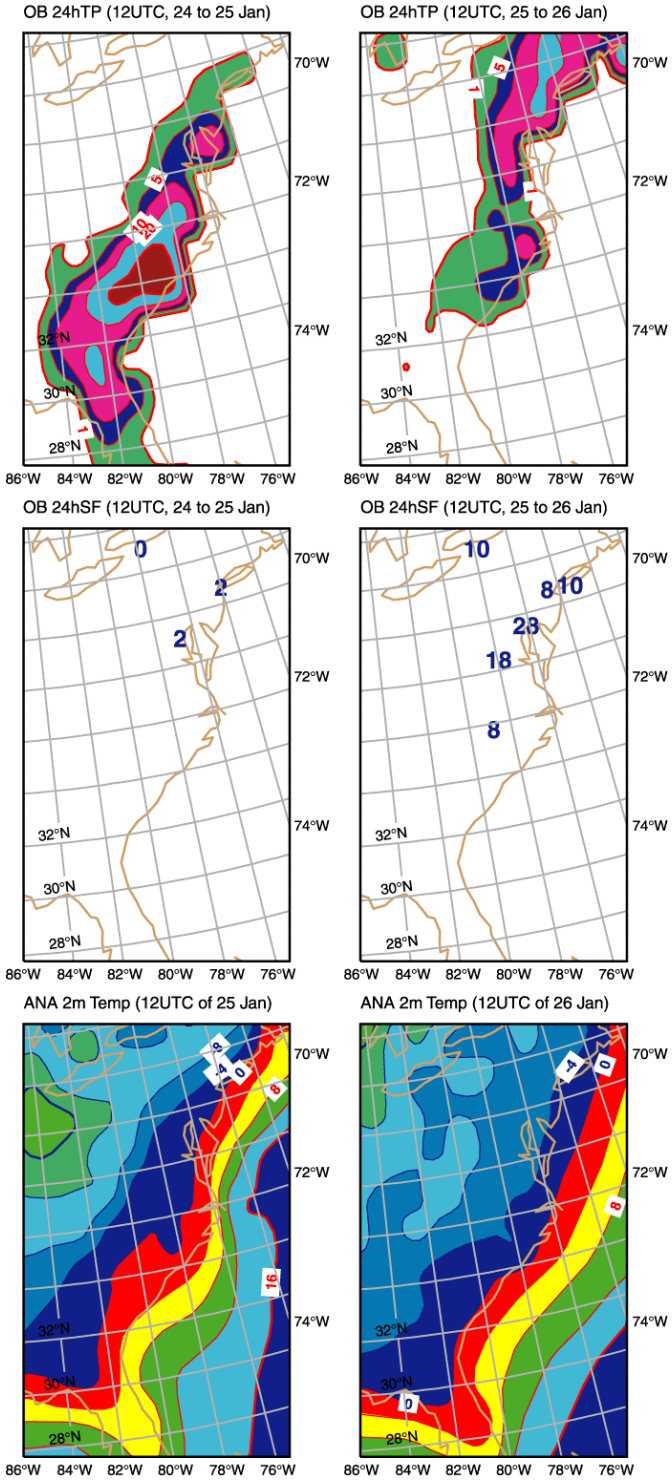

Figure 1. Observed precipitation accumulated (mm) between 12 UTC of (a) the 24th and the 25th and (b) the 25th and the 26th of January 2000 precipitation (data were kindly provided by *Steve Mullen*). (c-d) Observed snowfall (mm of equivalent water) at some stations of the East Coast (these are the station that reported snow-depth on the 24th, 25th and 26th of January with longitude between 80W and 70W and latitude between 30N and 50N) accumulated over the same period. (e) Observed 2m temperature (i.e. ECMWF analysis) at 12 UTC of the 25th. (f) as (e) but for the 26th. Contour isolines: 1, 5, 10, 20 and 40mm for precipitation, and every 2◦C for temperature.

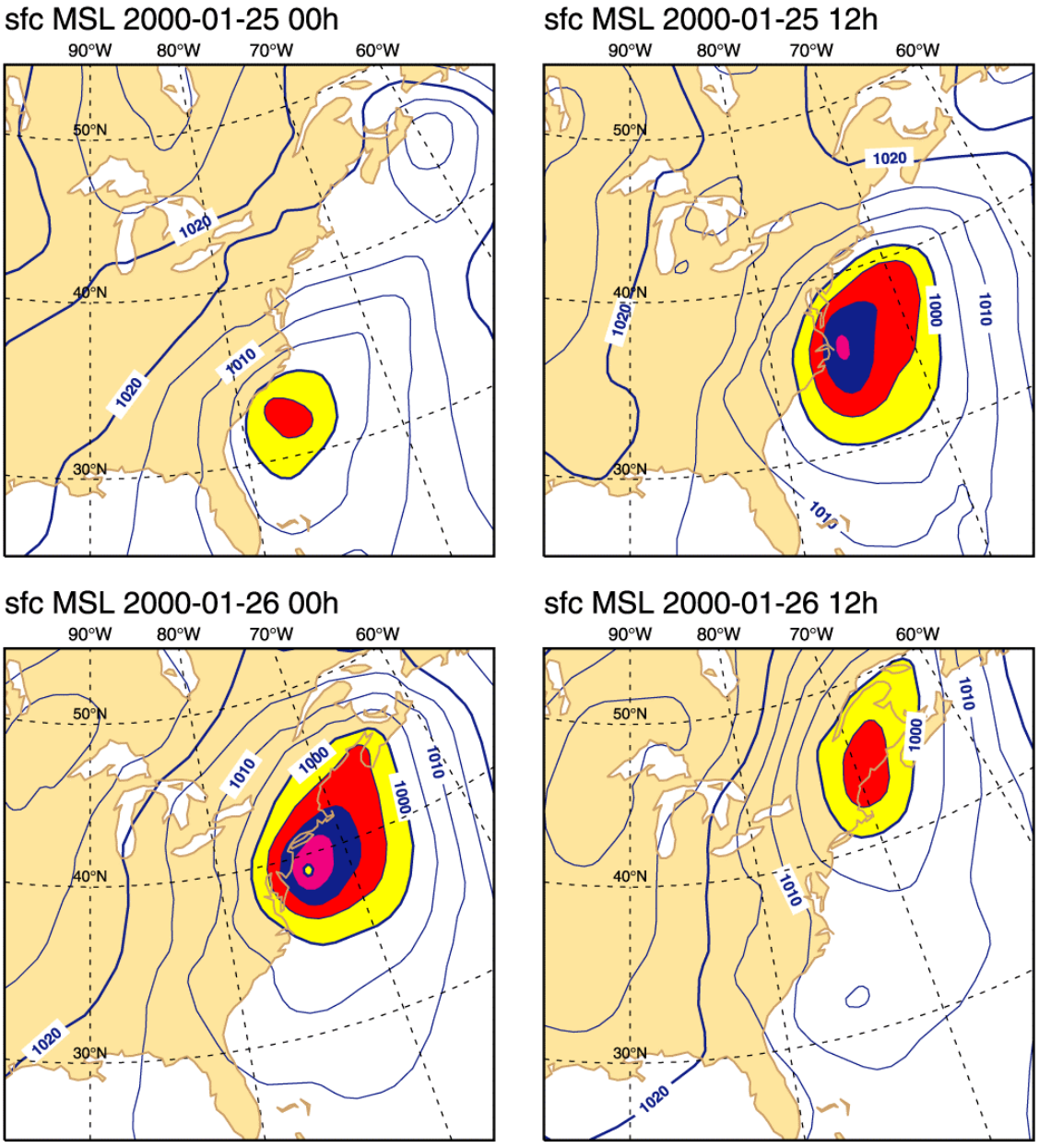

Figure 2. Mean-sea-level-pressure (a) at 00 UTC on the 25th, (b) at 12 UTC on the 25th, (c) at 00 UTC on the 26th and (d) at 12 UTC on the 26th. Contour interval 5 hPa.

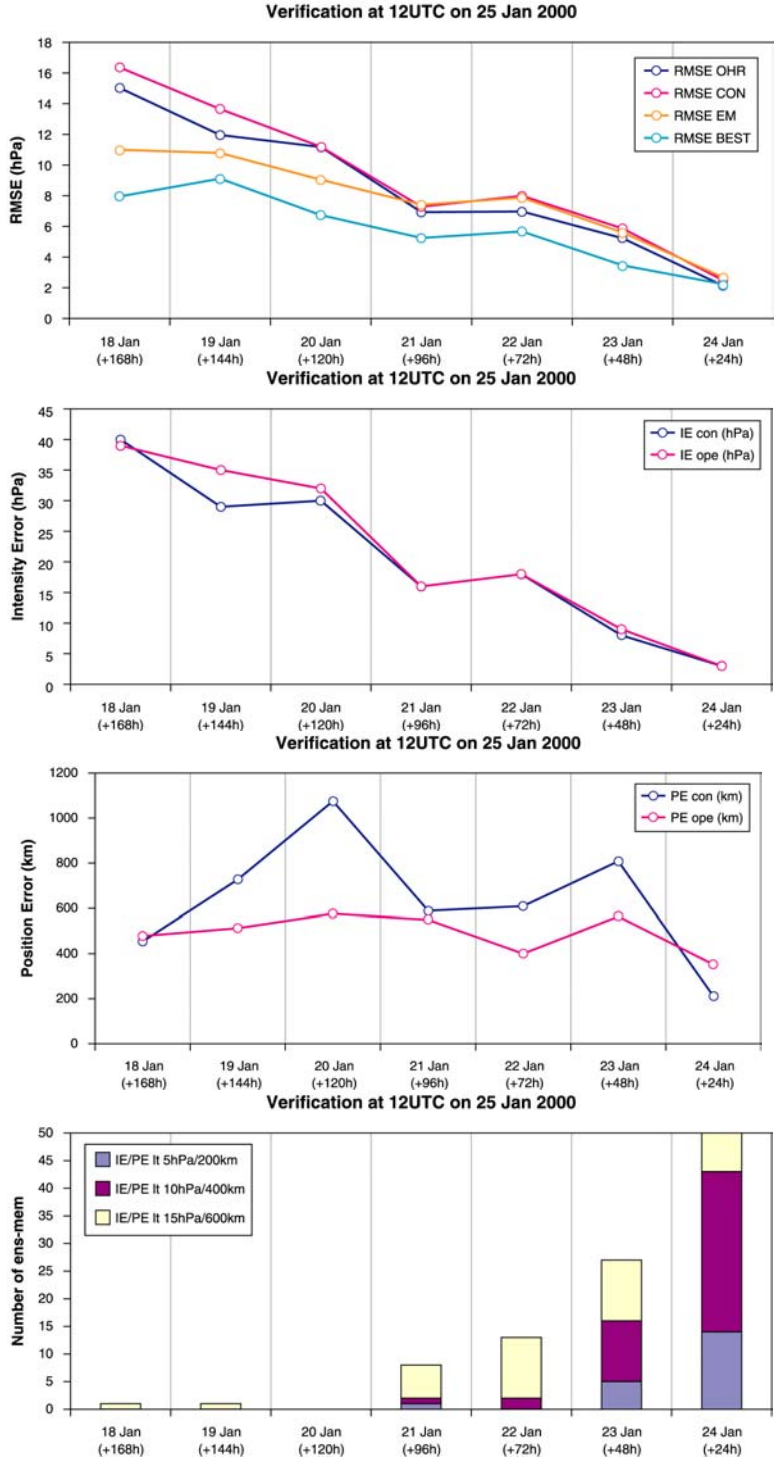

Figure 3. MSLP forecasts valid for 12 UTC of the 25th of January. (a) RMSE of the T_L319 operational high-resolution (OHR) model (solid line with diamonds), EPS control (dashed line with squares), ensemble-mean (dotted line with triangles) and best perturbed-member (chain-dashed line with crosses). (b) MSLP intensity error (IE, hPa) of the T_L319 operational high-resolution model (solid line with diamonds) and the EPS control (dashed line with squares). (c) as (b) but for the position error (PE, km). (d) number of EPS members with IE/PE smaller than 5hPa/200km (pattern with vertical lines), with IE/PE between 5hPa/200km and 10hPa/400km (pattern with squares) and with IE/PE between 10hPa/400km and 15hPa/600km (pattern with dots).

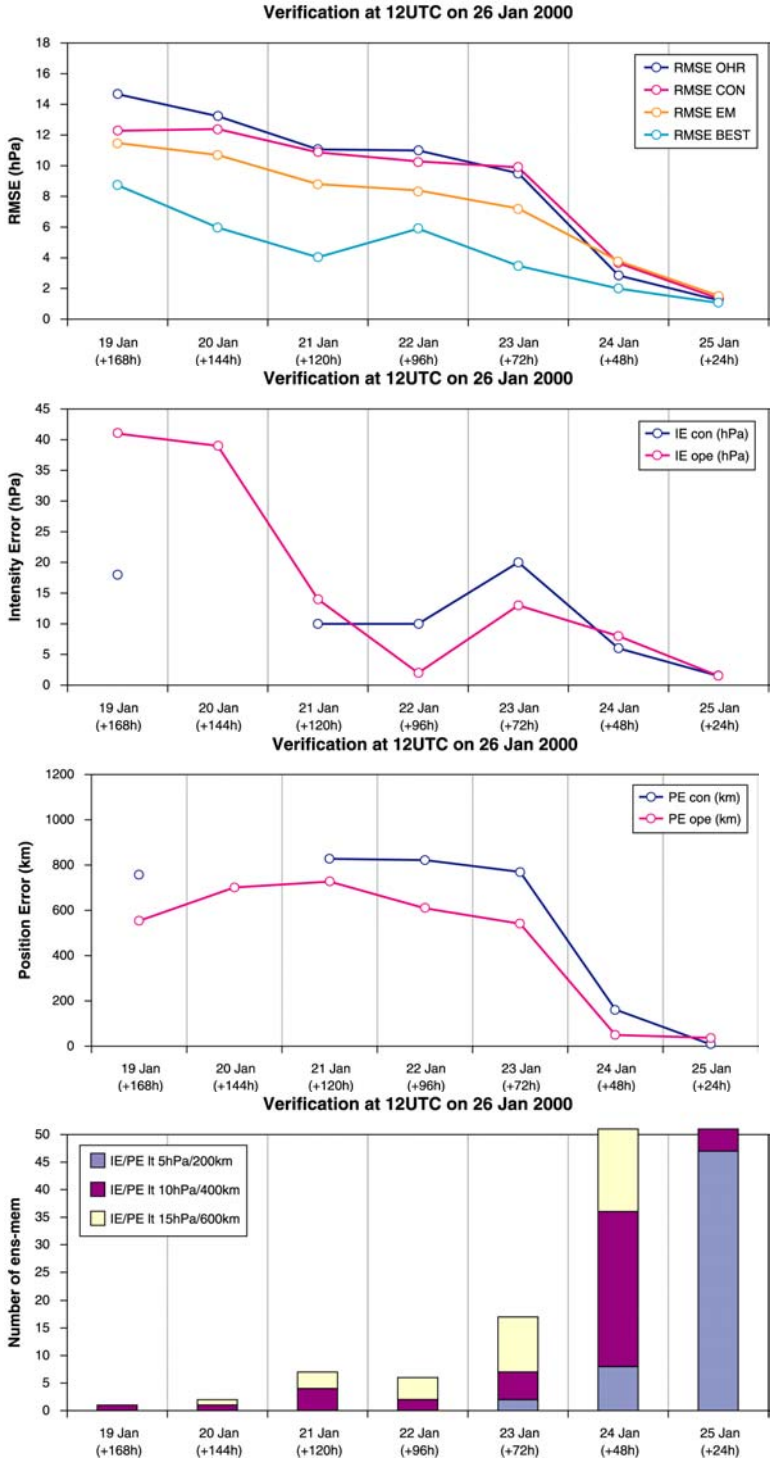

Figure 4. As Fig. 3 but for MSLP forecasts valid for 12 UTC of the 26th of January.

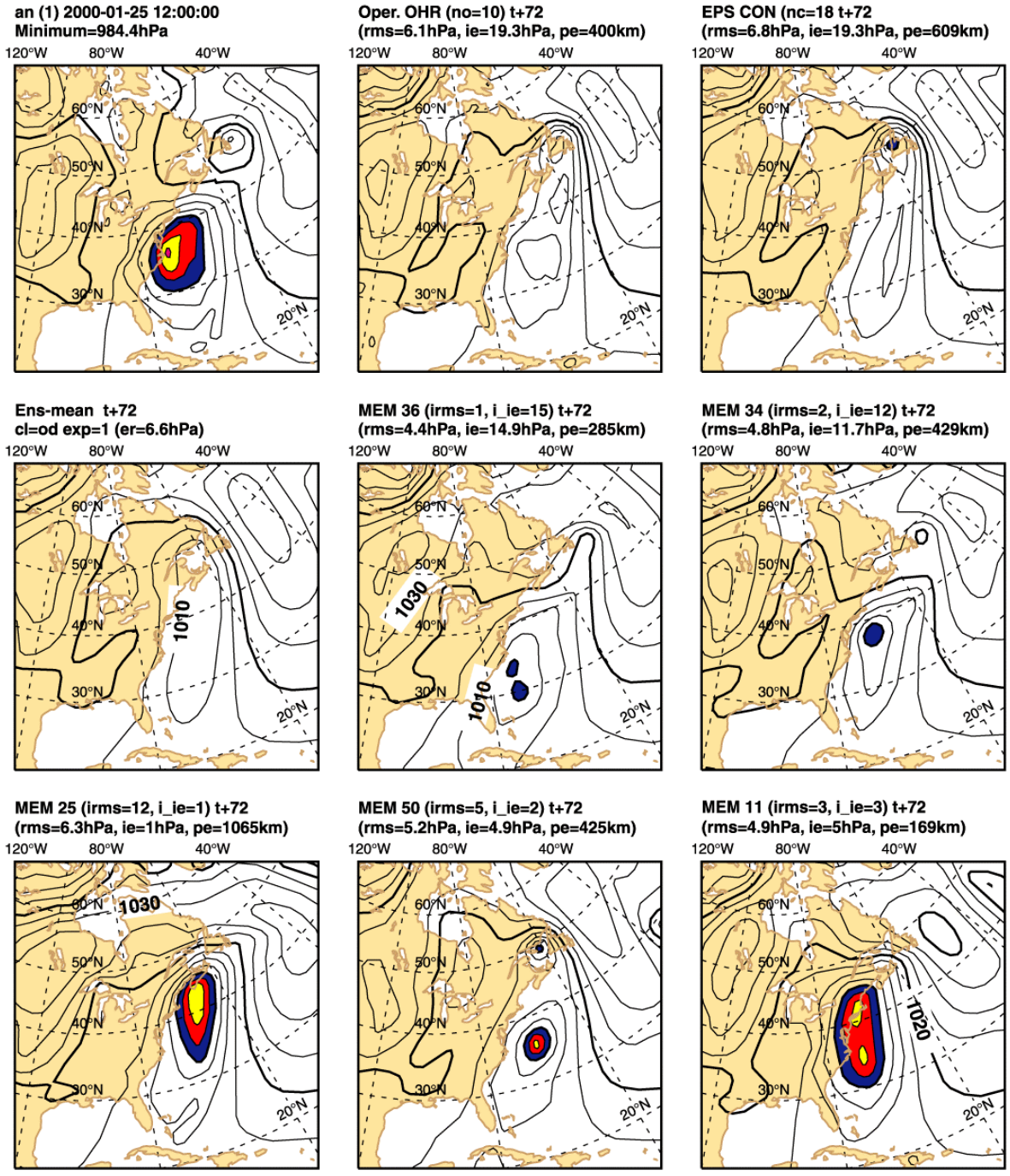

Figure 5. (a) MSLP verification valid at 12GMT on the 25th of January. Other panels: 72-h forecasts started on the 23rd of January: (b) operational high-resolution (OHR) T_L319, (c) EPS control, (d) 72-h ensemble-mean, (e) EPS member 36 (smallest rmse), (f) EPS member 34 (2nd lowest rmse), (g) EPS member 25 (lowest IE), (h) EPS member 50 (2nd lowest IE) and (i) EPS member 11 (3rd lowest IE). Contour interval is 5hPa. In the forecast titles, *rms* is the forecast RMSE, *ie* the intensity error and *pe* the position error; for the T_L319 *no* is the number of EPS perturbed-members with rmse smaller than the T_L319; for the EPS control *nc* is the number of EPS perturbed-members better than the control; for the EPS members, *irms* is the ranking position with respect to the 50 perturbed forecasts in terms of RMSE and *i_ie* is the ranking position in terms of IE.

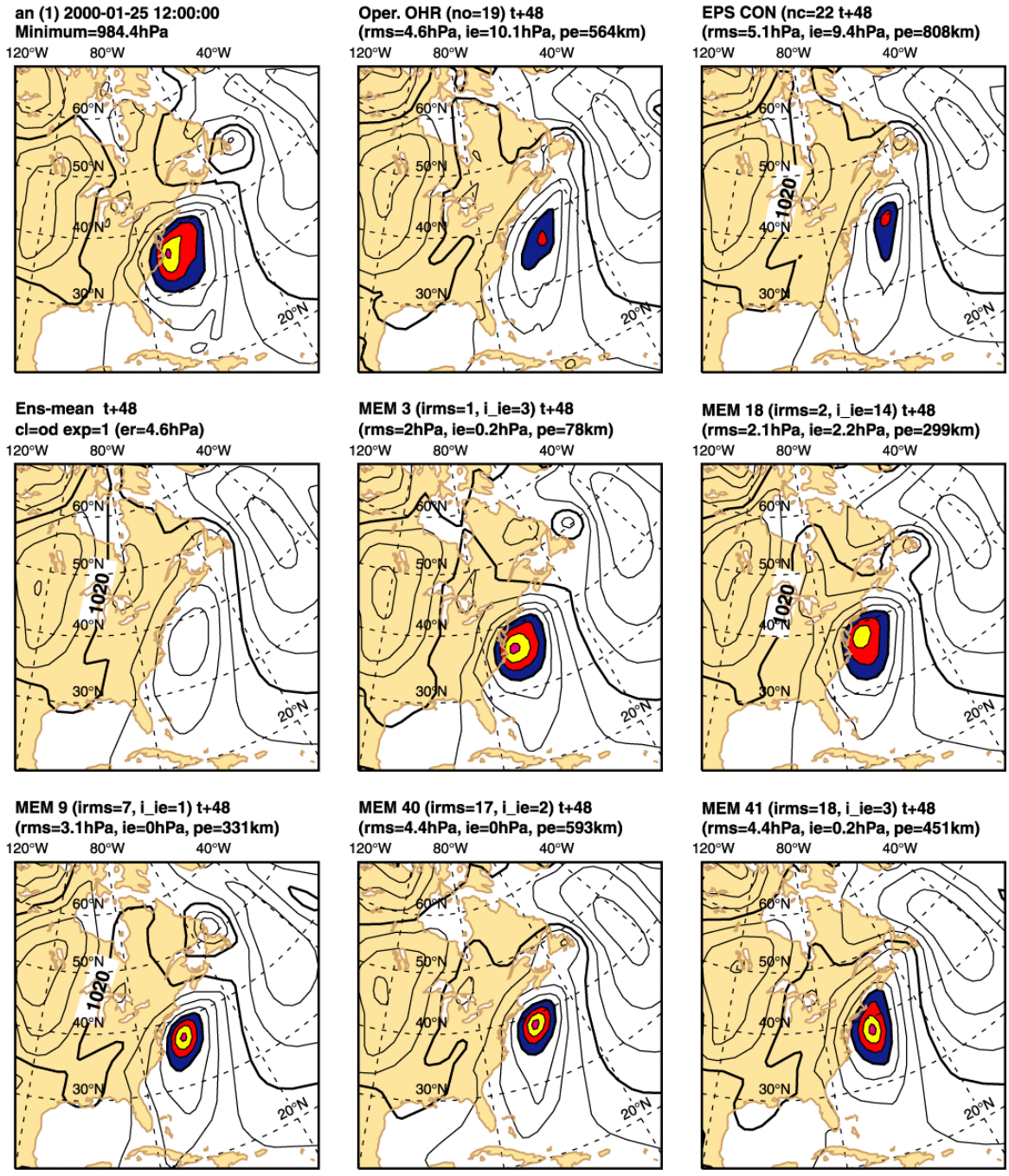

Figure 6. As Fig. 5 but for 48-h forecasts started on the 22nd and valid for the 25th of January.

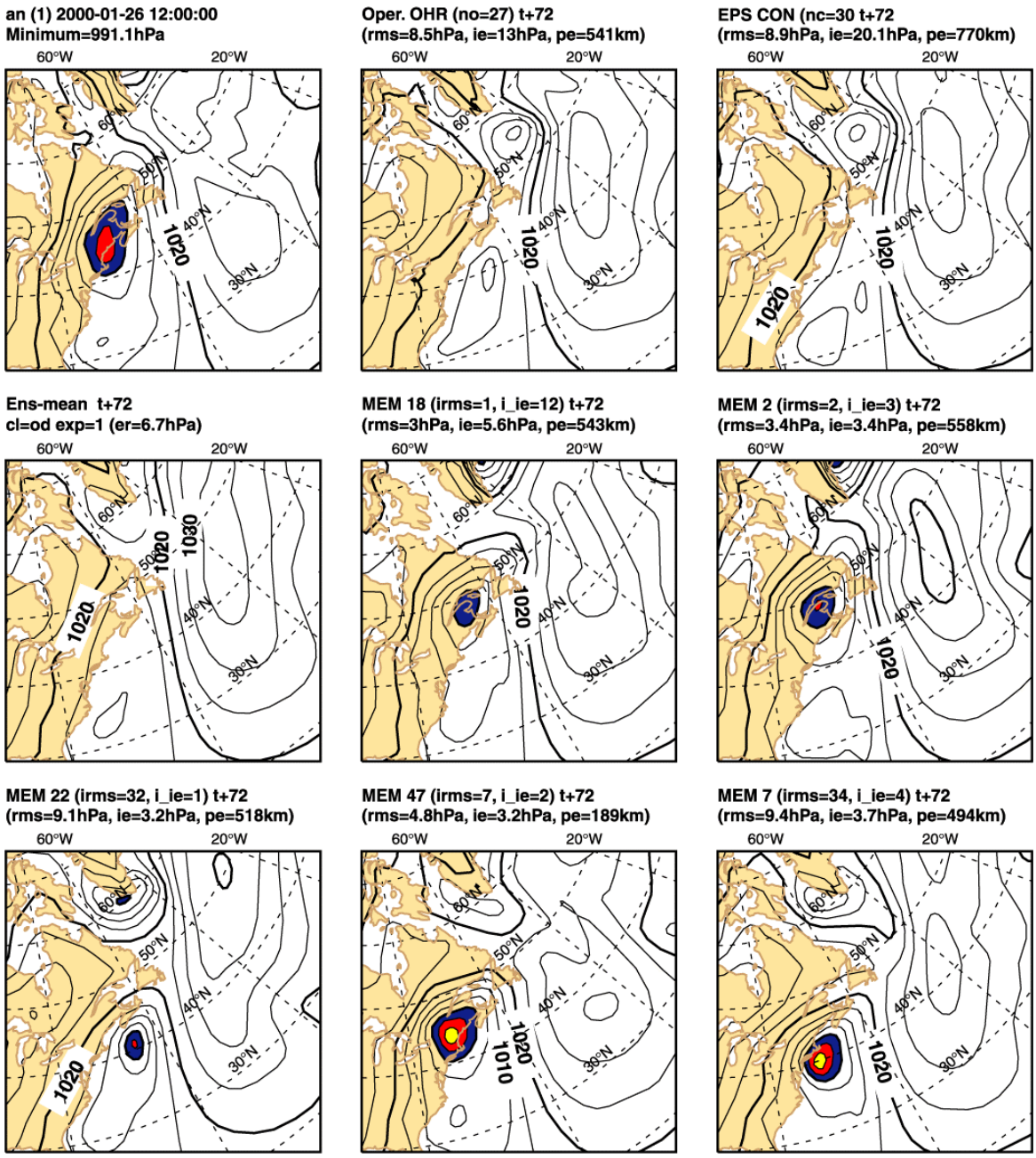

Figure 7. As Fig. 5 but for 72-h forecasts started on the 23rd and valid for the 26th of January.

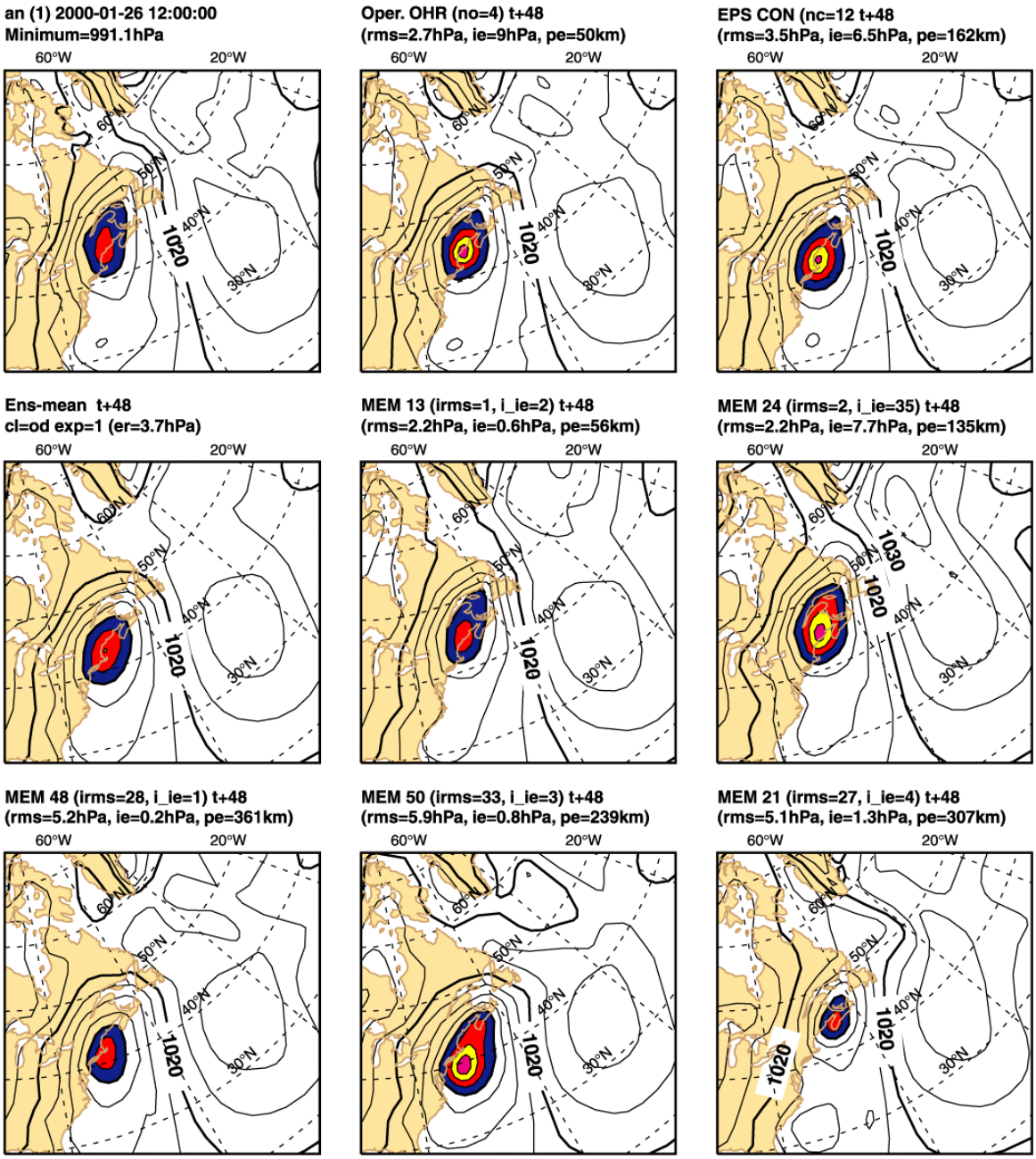

Figure 8. As Fig. 5 but for 48-h forecasts started on the 23rd and valid for the 26th of January.

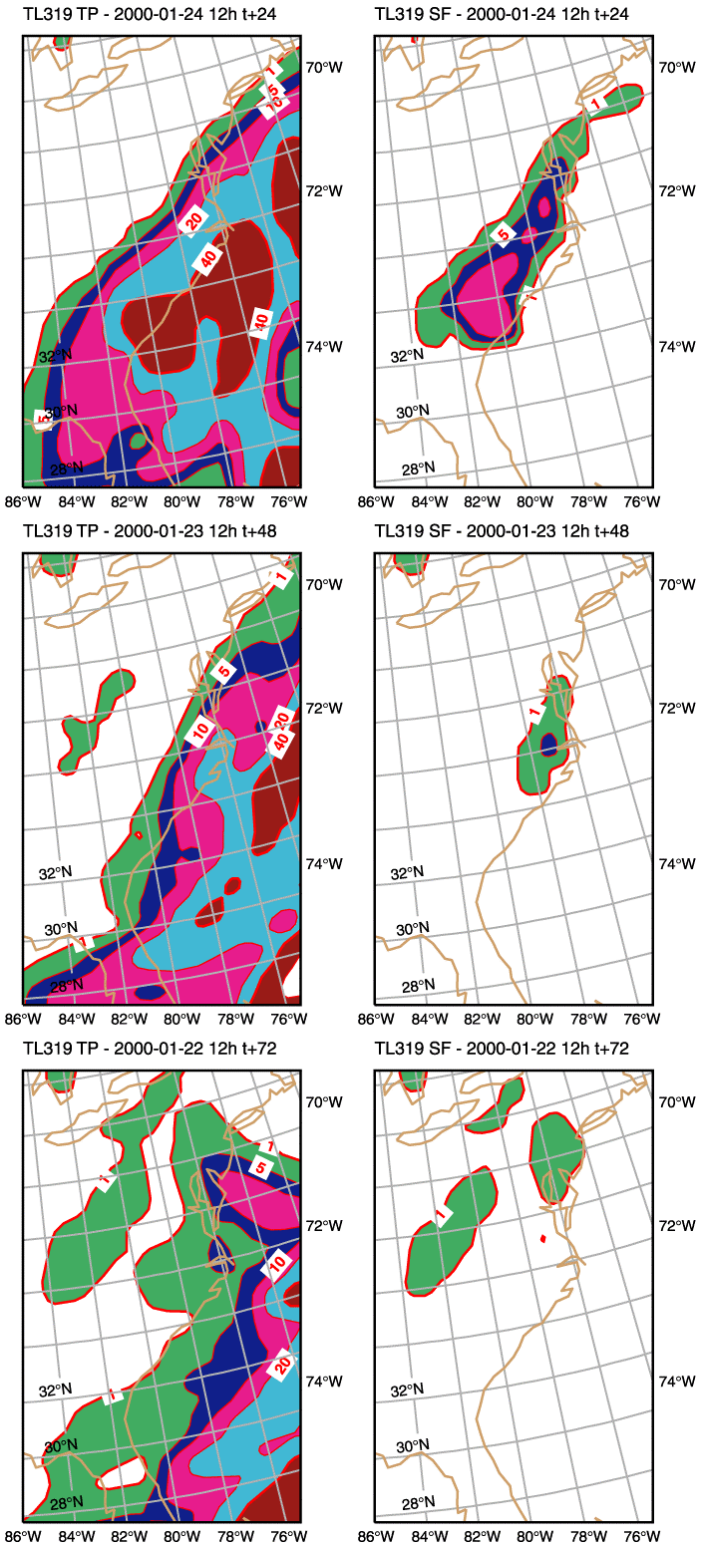

Figure 9. Snowfall (left panels) and total precipitation (right panels) forecasts valid for fields accumulated between 12 UTC of the 24th and the 25th of January (observed fields are shown in Figs. 1a and 1c). (a) T_L319 24-h snowfall forecast started on the 24th. (b) as (a) but for total precipitation. (c-d) as (a-b) but for the t+48-h forecasts started on the 23rd. (e-f) as (a-b) but for the 72-h forecasts started on the 22nd. Contour isolines: 1, 5, 10, 20 and 40 mm.

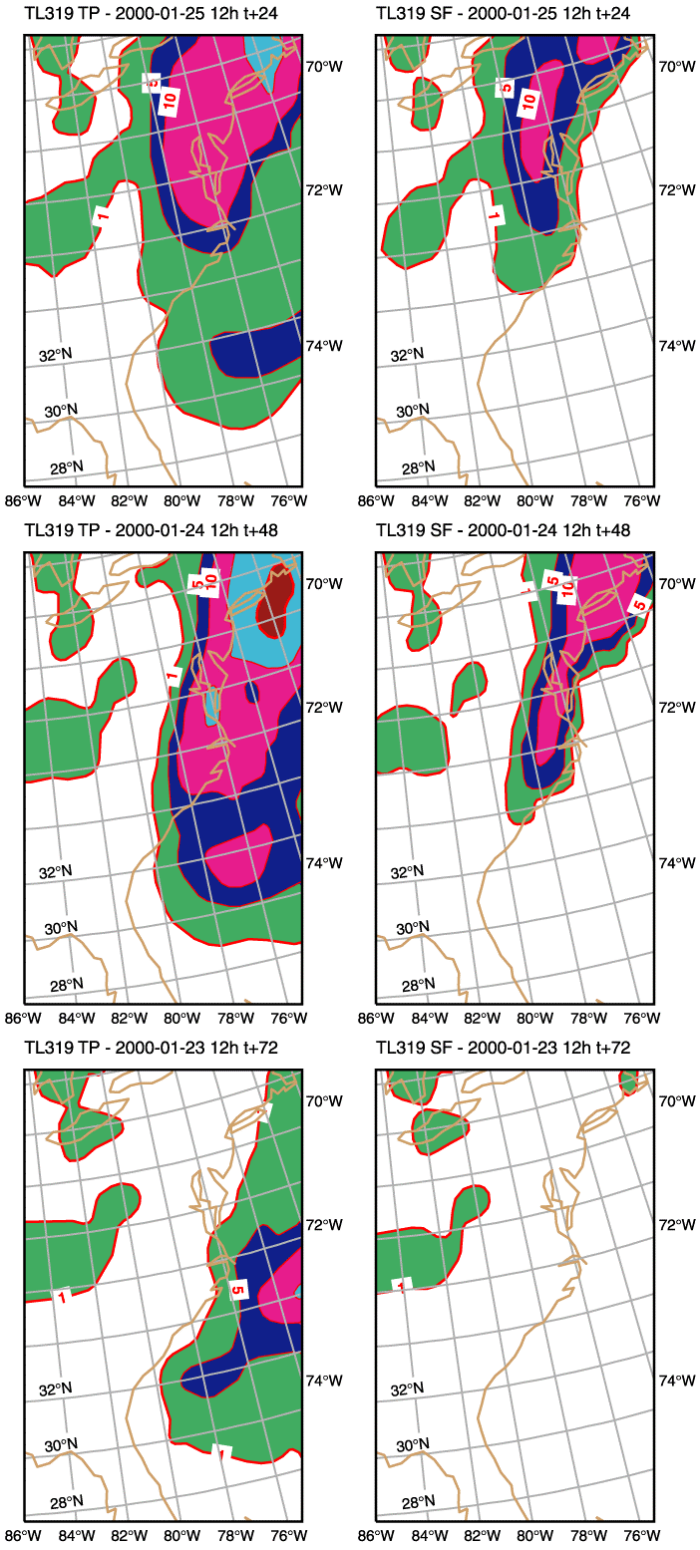

Figure 10. As Fig. 9 but for fields accumulated between 12 UTC of the 25th and the 26th of January (observed fields are shown in Figs. 1b and 1d).

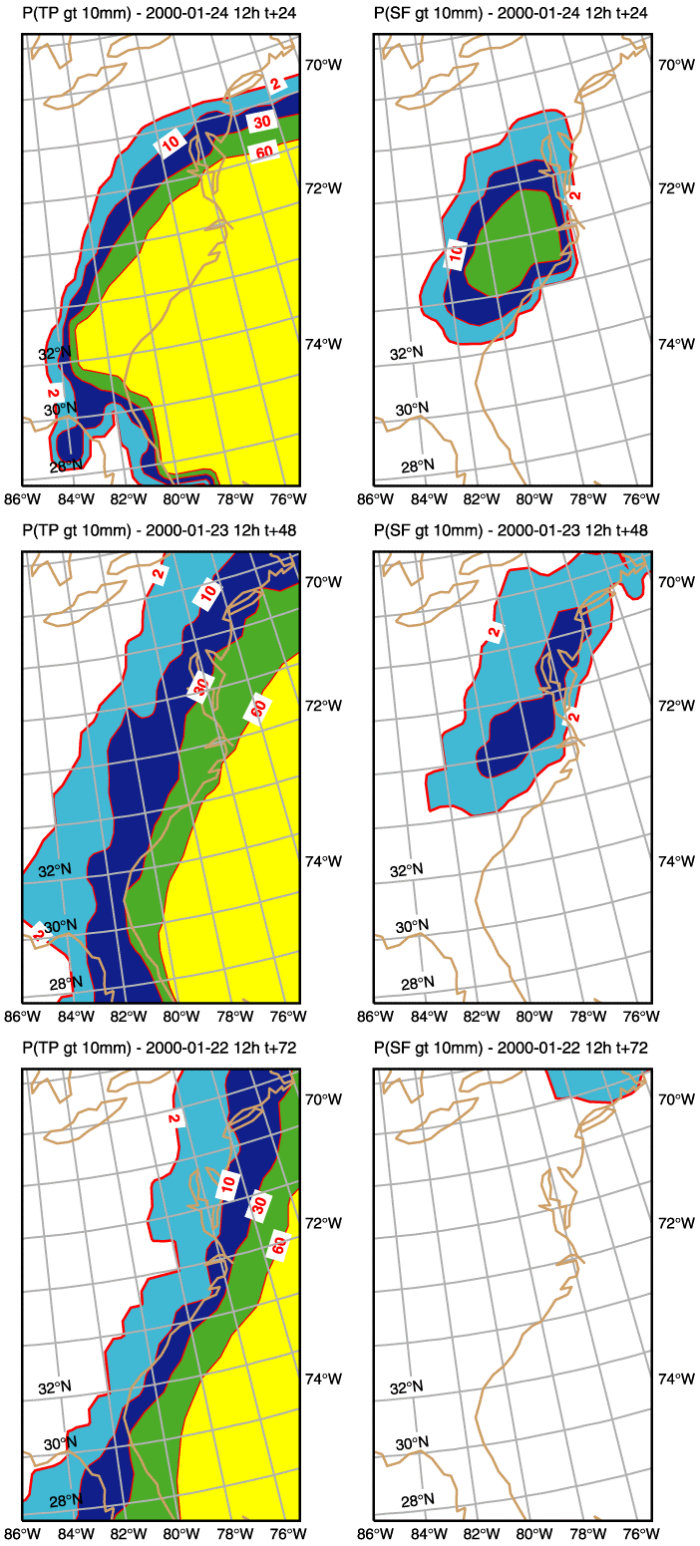

Figure 11. (a) Probability of '24-h precipitation in excess of 10mm' predicted on the 24th and valid from 12 UTC of the 24th to 12 UTC of the 25th. (b) as (a) but for snowfall. (c): as (a) but for the 48-h predictions started on the 23rd. (d): as (c) but for snowfall. (e): as (a) but for the 72-h prediction started on the 22nd. (f): as (e) but for snowfall. Contour isolines: 2, 10, 30 and 60%.

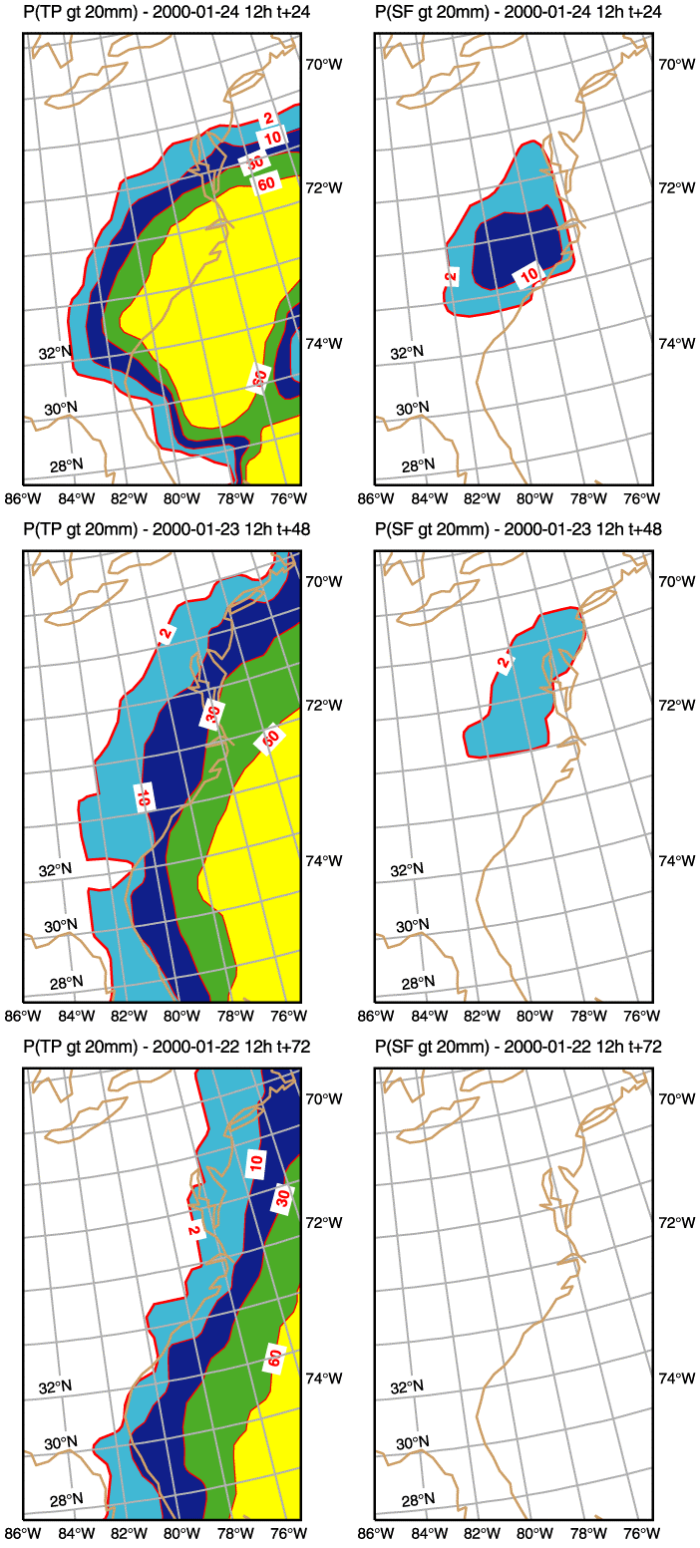

Figure 12. As Fig. 11 but for the event '24-h precipitation in excess of 20mm'.

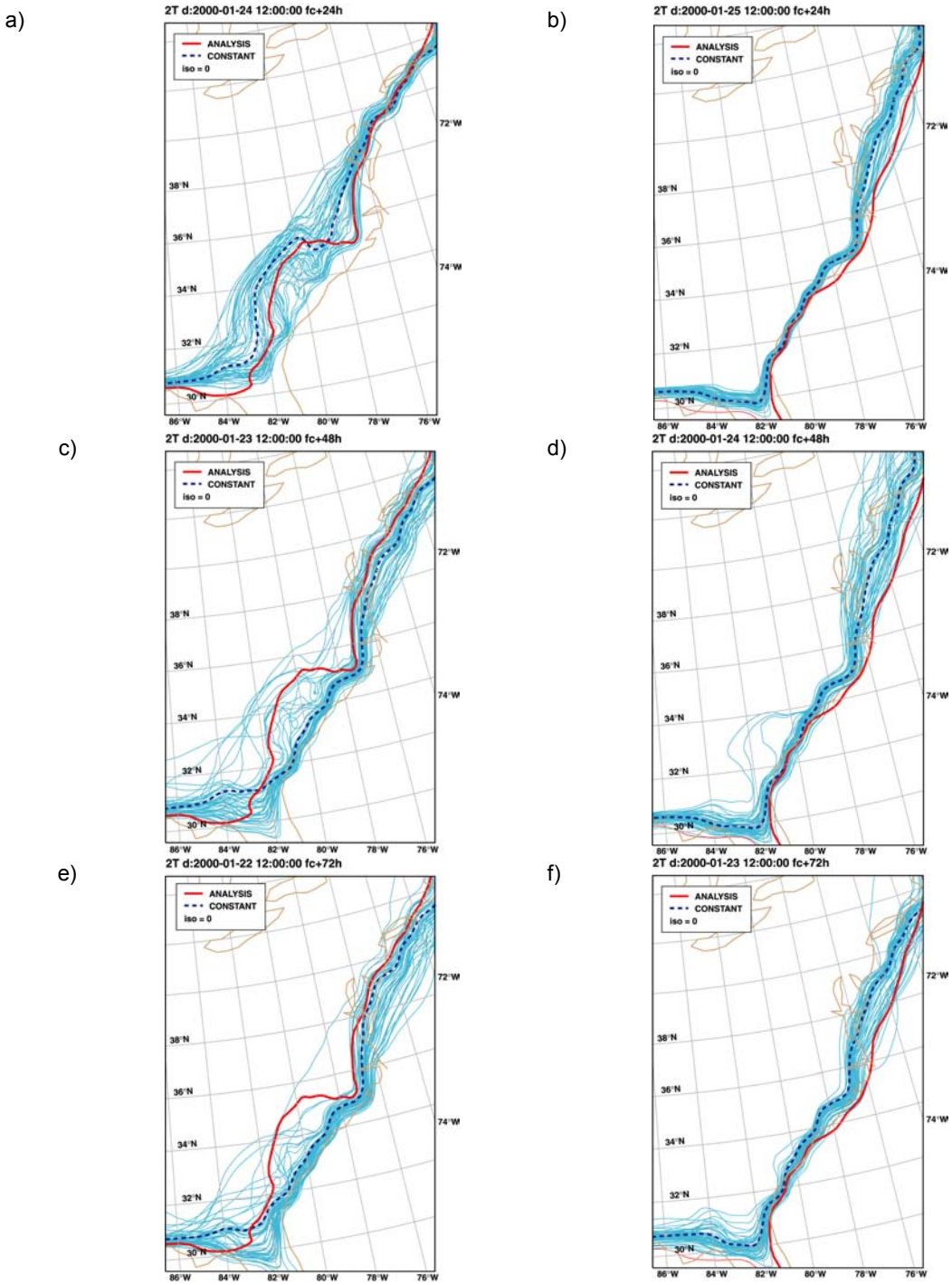

Figure 13. Observed (i.e. analysis, solid bold) and forecast by the EPS control (dash bold) and perturbed members (solid thin) position of the 0◦C isotherm for 2m temperature:

(a) 24-h forecast issued on the 24th and analysis for 12UTC of the 25th;
(b) 24-h forecast issued on the 25th and analysis for 12UTC of the 26th;
(c) 48-h forecast issued on the 23rd and analysis for 12UTC of the 25th;
(d) 48-h forecast issued on the 24th and analysis for 12UTC of the 26th;
(e) 72-h forecast issued on the 22nd and analysis for 12UTC of the 25th;
(f) 72-h forecast issued on the 23rd and analysis for 12UTC of the 26th.
The latitude/longitude grid spacing is 2 degrees.

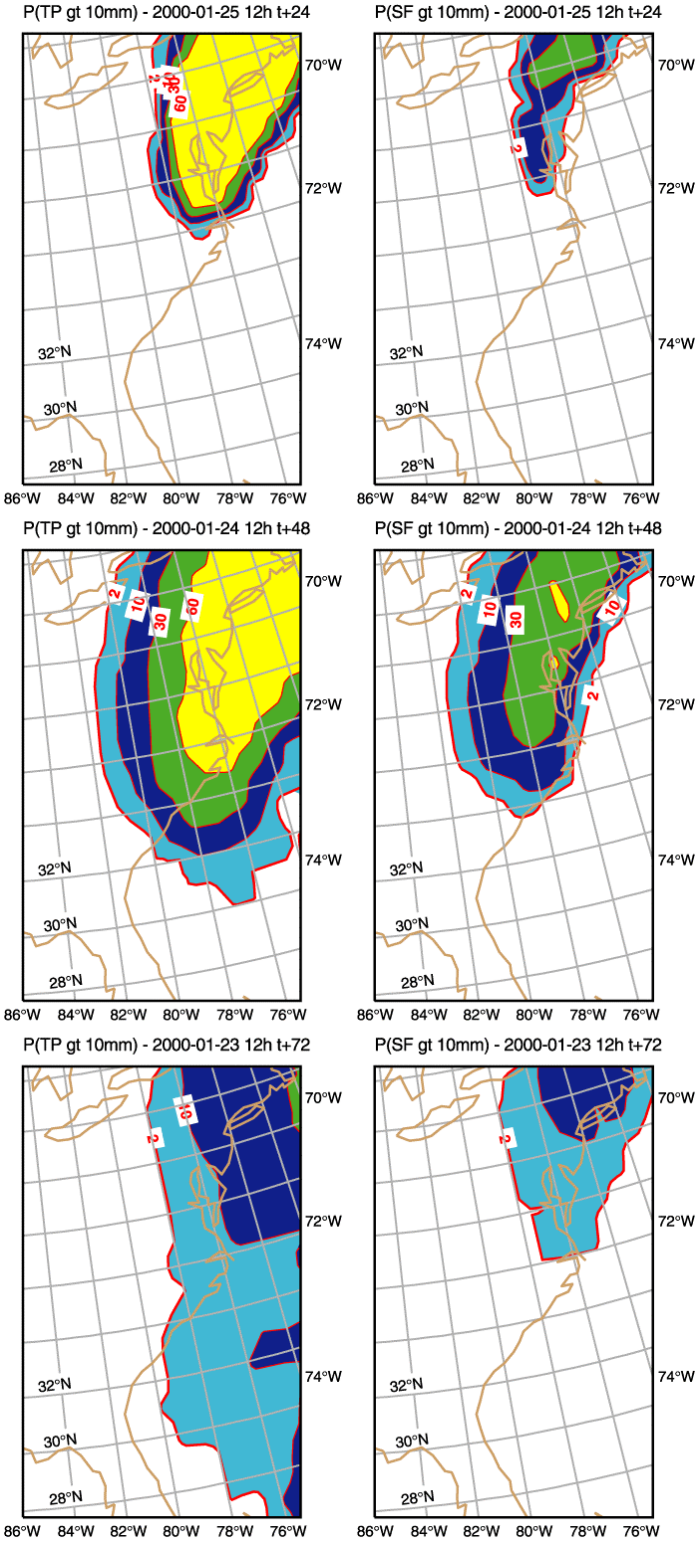

Figure 14. (a) Probability of '24-h precipitation in excess of 10mm' predicted on the 25th and valid from 12 UTC of the 25th to 12 UTC of the 26th. (b) as (a) but for snowfall. (c): as (a) but for the 48-h predictions started on the 24th. (d): as (c) but for snowfall. (e): as (a) but for the 72-h prediction started on the 23rd. (f): as (e) but for snowfall. Contour isolines: 2, 10, 30 and 60%.

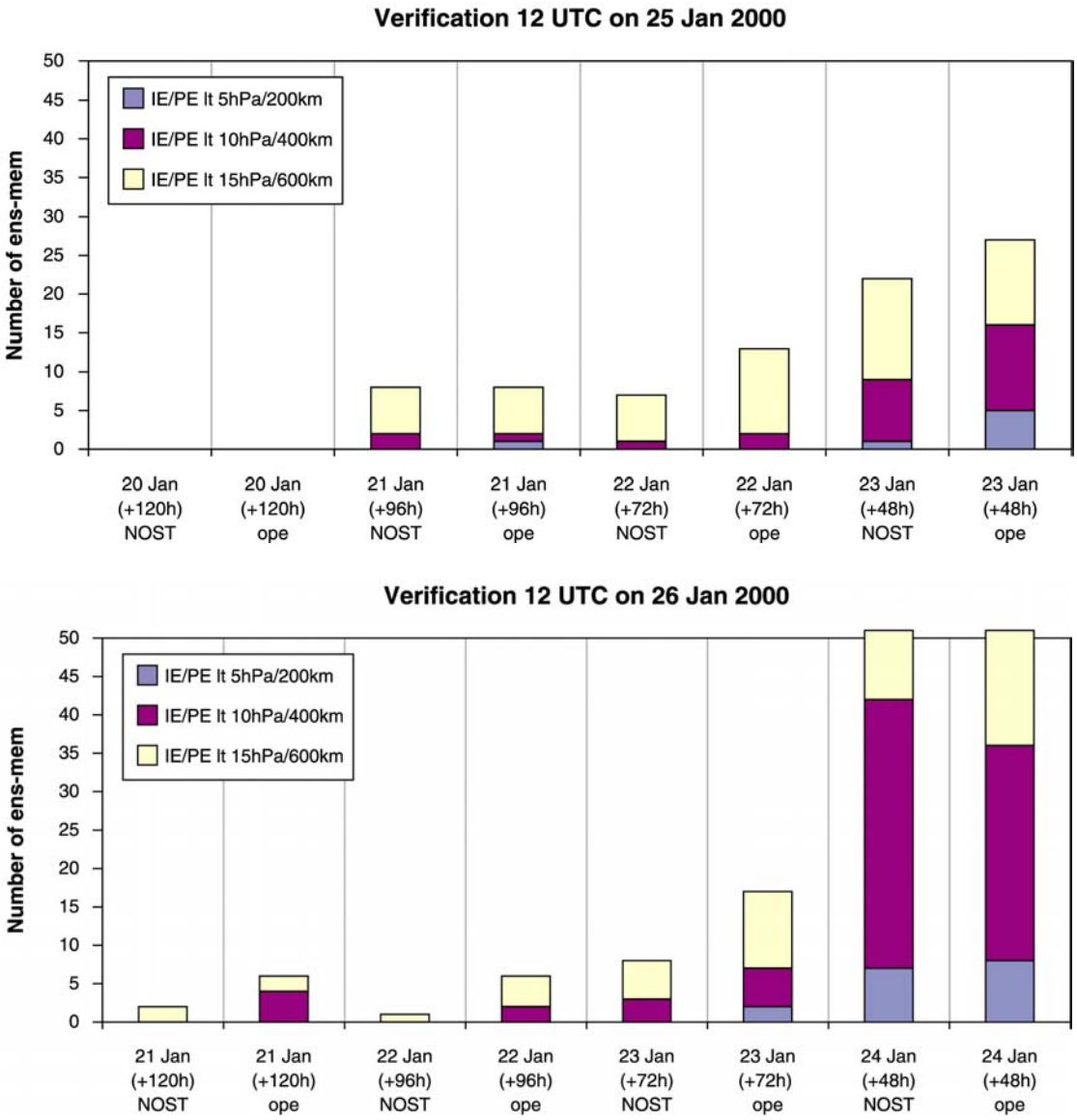

Figure 15. Number of MSLP perturbed-member forecasts with IE/PE smaller than 5hPa/200km (pattern with vertical lines), with IE/PE between 5hPa/200km and 10hPa/400km (pattern with squares) and with IE/PE between 10hPa/400km and 15hPa/600km (pattern with dots) for EPS and NOST-ensemble forecasts with different lead times: (top) for forecasts valid for 12 UTC of the 25th and (bottom) of the 26th of January.

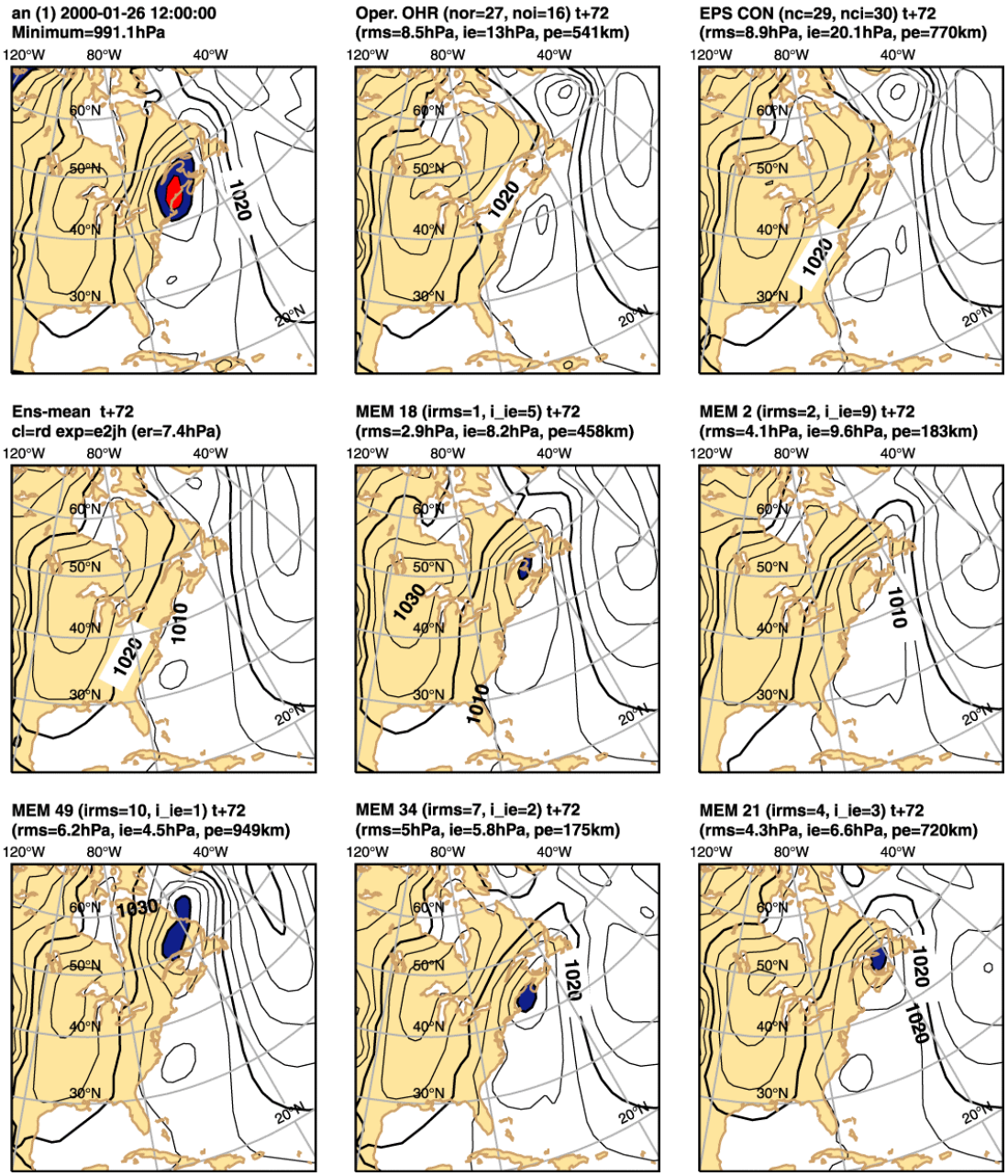

Figure 16. As Fig. 5 but for 72-h NOST-ensemble forecasts started on the 23rd and valid for the 26th of January.

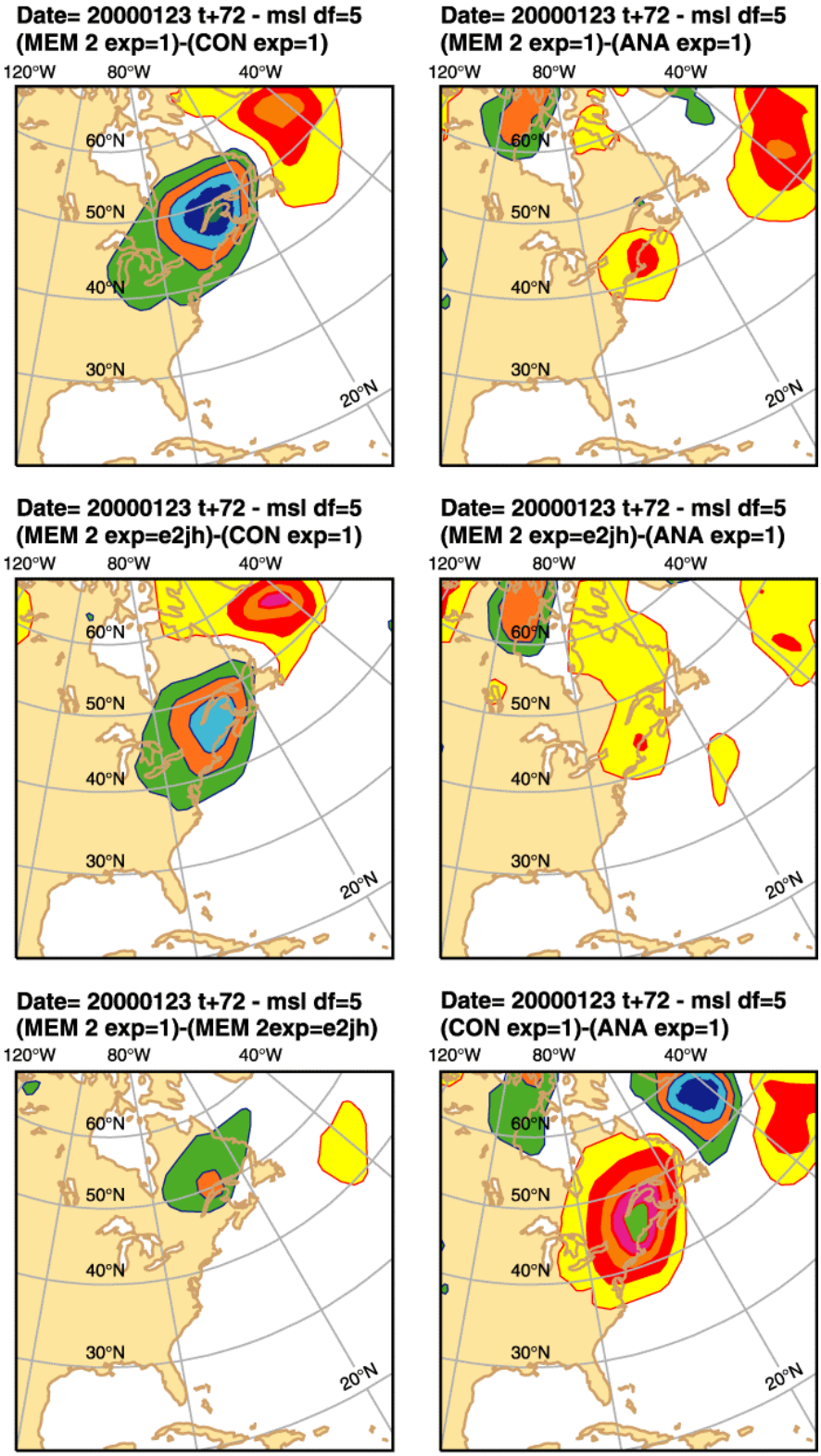

Figure 17. MSLP 72-h forecasts started on the 23rd and valid for 12 UTC of the 26th of January: (a) difference (EPS2-CON), (b) error (EPS2-ANA), (c) difference (NOST2-CON), (d) error (NOST2-CON), (e) difference (EPS2-NOST2) and (f) error (CON-ANA). Contour interval 5hPa, with positive (negative) values in yellow-red (green-blue).

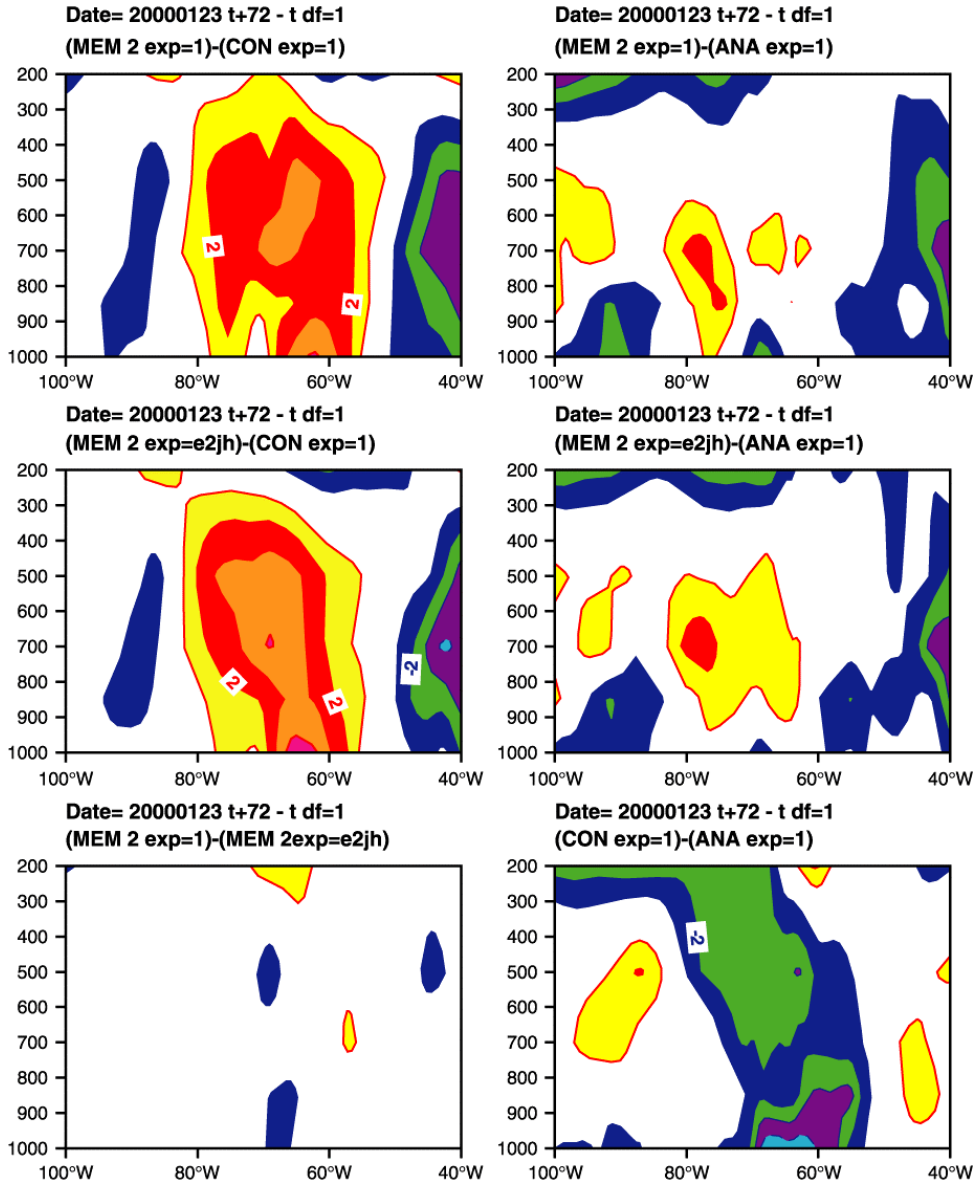

Figure 18. As Fig. 17 but for vertical cross section (longitude-height) of temperature differences averaged between 30N-60N. Contour interval: 1 degree (solid/dash for above/below 0ºC).

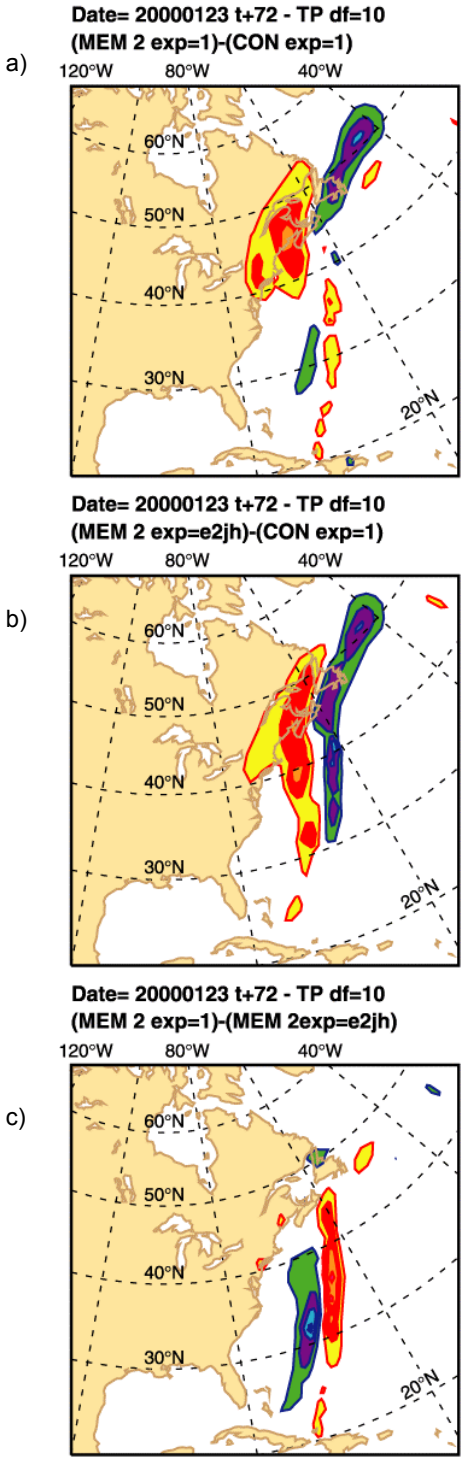

Figure 19. Total precipitation accumulated between t+48h and t+72h for forecasts started on the 23rd and valid for 12 UTC of the 26th of January: (a) difference (EPS2-CON), (b) difference (NOST2-CON) and (c) difference (EPS2-NOST2). Contour interval 10 mm, (solid/dash for positive/negative values).